THE STRUCTURE OF COMPACT RADIO SOURCES AT 10.7 GHz

Thesis by

David Bruce Shaffer

In Partial Fulfillment of the Requirements

for the Degree of

Doctor of Philosophy

California Institute of Technology

Pasadena, California

1974

(Submitted September 25, 1973)

To

Suzie

Not to

Los Angeles

ACKNOWLEDGMENTS

I would never have discovered radio astronomy but for the NRAO Summer Student program. To NRAO (personified by Bill Howard), Ken Kellermann, Ivan Pauliny-Toth, and Mike Davis go the credit for introducing an ignorant physics major into the ways and wonders of radio telescopes and radio sources.

Marshall Cohen continued the nurturing as an enthusiastic West Coast advisor. Between trips to Mt Whitney and Kings Canyon, he guided me through the intricacies, joys, and sorrows (you would not believe the number of things that can go wrong with an experiment!) of long baseline interferometry.

A VLB experiment is always a team project since it requires a minimum of two telescopes and two observers. An experiment like this one actually requires the active cooperation of many people. Perhaps first and foremost are the generally unsung telescope and electronics staffs. To them go sincere appreciation for making it all work. I thank the observatory directors for the allotment of observing time. Special thanks go to those who actually helped observe: Ken Kellermann and George Grove at NRAO; Ron Rinehart and Dick Ellis at HRAS; and Marshall Cohen and Al Moffet at OVRO. (In case the reader thinks I didn't do anything, I was at HRAS.)

George Purcell deserves special mention for enlightening

discussions about the Mark II system. Barry Clark, George Grove, Frank Willoughby, Benno Rayhrer, and Joe Burch kept the Mark II processor functioning. Without them, I'd have only $\sim 2 \times 10^{12}$ bits of useless information.

I thank Bryan Andrew, Bill Dent, and Ron Ekers for unpublished flux density measurements. The Anglo-Canadian VLB group supplied pre-publication information about the 2.8 cm structure of 3C 84 and OJ 287. John Broderick, Michael Yerbury, Dave Jauncey, and Ken Kellermann provided interesting (and even useful) 13 cm VLB data.

My literary talents (?) were finely honed by a brief stint as a member of the editorial board of "The Journal of the Pocahontas County Astronomical Society", which I promised to mention in my thesis.

Suzie Robinson and Barbara Ellis are thanked for their typing efforts.

Last, but not least, the National Science Foundation paid for all this. Receipt of four years of Fellowship and one year of Traineeship aid are gratefully acknowledged.

ABSTRACT

Very long baseline interferometry has been used to study the compact structure of seven radio sources at 10709 MHz (λ = 2.8 cm). The observations, the first of a series, were made on April 28 - May 1, 1972, using the NRAO Mark II recording system. Antennas of the Owens Valley Radio Observatory (California), the Harvard Radio Astronomy Station (Texas), and the National Radio Astronomy Observatory (West Virginia) were used to give three baselines that greatly improved the (u,v)-plane coverage compared to the coverage of previously used single baselines. The three baselines had lengths of 119, 84, and 54×10^6 λ.

The observed sources were 3C 84, NRAO 150, OJ 287, 4C 39.25, 3C 273, PKS 2134+004, and VRO 42.22.01 (BL Lac). They were tracked by all three antennas during the time of mutual visibility, giving 8 to 11.5 hours of continuous coverage. With the maximum baseline of 119×10^6 λ and a u-v cell size of $\sim 40 \times 10^6$ λ, it is unlikely that we have missed any important structure information in the range 0".0005 to 0".005.

Fourier inversion of the observations was impossible because there was no phase calibration, and model fitting procedures were used to interpret the data. For five of the sources (NRAO 150, OJ 287, 4C 39.25, 3C 273, and VRO 42.22.01)

models were found that fit the observations quite well. For 3C 84 and PKS 2134+004 no simple model could be found, but a rough idea of the source structure was still possible. For most of the sources, interferometric results at other frequencies and resolutions are consistent with the present findings, and a joint interpretation is given.

For all the sources except OJ 287 (which looks like a point source at our resolution and was used to calibrate the correlated flux density scale) and possibly NRAO 150, two or more separate components are required to match the observations. Component separations range from 0".0006 to 0".005 and their sizes from $\lesssim$0".0003 to $\sim$0".002. Components less than $\sim$0".002 contribute 0.85 or more of the total 10.7 GHz flux density for all the sources. Assuming synchrotron self-absorbed components, the magnetic fields in the compact sources are $\sim 10^{-3\pm1}$ gauss. This value is less than the equipartition field, and the individual components are expected to expand from particle pressure.

Suggestions are given for additional observations to improve our knowledge of the structure and nature of compact sources.

TABLE OF CONTENTS

Chapter 1. Introduction

One of the long-standing objectives of radio astronomy has been high angular resolution. To compare radio and optical features, a resolution of about one arc-second is desirable. Still higher resolution is necessary to study the origin and evolution of the most compact radio sources. Even one arc-second observations, however, require antenna sizes of many kilometers at centimeter wavelengths. This is obviously an impossible size for a single antenna, so it is necessary to operate two or more antennas together as an interferometer for the highest resolution.

A standard radio interferometer consists of antennas connected by cables that carry local oscillator (LO) reference signals to the antennas and bring back the intermediate frequency signal to a central processing location. (See Read (1963) for a description of such a system.) These interferometers (with several antennas separated by several kilometers) now give the best radio pictures available, with angular resolutions approaching a second of arc (Ryle 1972). Such systems measure the amplitude and phase of the Fourier transform of the radio source brightness distribution. The data may then be inverted to recover the brightness distribution. A cable-connected interferometer is limited in size (and thus angular resolution) by the expense, complexity and stability of the interconnections.

Essentially all radio astronomical receiving systems use a local oscillator to heterodyne the high frequency signal band down to a low frequency video signal that is easier to amplify and detect. In an interferometer, this LO must be coherent at the several antennas in order to maintain the coherence of the received signals before they are added or multiplied. A phase-stable LO reference signal is usually carried about by cable, as noted above. In order to increase the interferometer baseline to many kilometers (hundreds or thousands), a different way must be found to present a coherent LO signal to the receivers. One method is to use microwave radio links. Elgaroy et al. (1962) describe such a system, and Palmer et al. (1967) give results at an angular resolution of $\sim$0".025. Again, however, there are practical limitations to the baseline lengths achievable.

Evidence from radio source spectra (Shklovskii 1965) and time-varying intensities (Dent 1965) indicated that resolutions much higher than 0".01 would be useful. At about the same time, atomic oscillators of sufficient stability to act as the coherent LO reference became available. Thus, it was possible to operate an interferometer with no real-time links between the antennas. The video signal could be recorded on magnetic tape for later analysis. Two recording schemes were developed, one analog (Broten et al.

1967), and one digital (Bare et al. 1967).

The early very long baseline interferometer (VLB) experiments proved the existence of compact radio sources. For the first several years of VLB observations, various experiments at higher and higher resolution were performed by using longer baselines and higher frequencies (shorter wavelengths) in order to make λ/d as small as possible.

Except for some work at $\lambda \simeq 70$ cm (Broten et al. 1969, Clarke et al. 1969), there were few attempts at systematic measurements of compact source brightness distributions. Usually, only one or two points of the visibility function were sampled, and a circular Gaussian approximation to the source structure was the given result.

As the byproduct of a relativity experiment, Knight et al. (1971) discovered the first compelling evidence for rather complex structure in two quasars (3C 273 and 3C 279) at the 10^{-3} arc-second level. Astoundingly, the apparent structure was found to change at a rapid rate (Whitney et al. 1971; Cohen et al. 1971). 3C 120, an N galaxy, was soon found to display similar behavior (Shaffer et al. 1972).

The interpretation of these single baseline (Goldstone-Haystack) observations depends heavily on model fitting, unavoidably guided by the modeller's prejudices. Such fitting, expecially to data from only one baseline, requires skill and daring and may be ambiguous (Cohen et al. 1971;

Shaffer et al. 1972) or even wrong. To improve this situation, more data from more baselines are desirable. To this end, we (M.H. Cohen, K.I. Kellermann and myself) decided to undertake a series of observations using three antennas (giving three baselines). It is the first of this series that is discussed in this thesis. These observations were made during 28 April - 1 May, 1972, at an observing frequency of 10609 MHz.

Chapter 2. The Observations

A. Choice of antennas and observing frequency

Before assembling the necessary equipment (tape recorders, atomic standards, etc.), we had to decide where to put it and what observing frequency to use. Since the principal investigators came from the Owens Valley Radio Observatory (OVRO, Big Pine, California) and the National Radio Astronomy Observatory (NRAO, Green Bank, West Virginia), the 40-m (130-foot) and 43-m (140-foot) antennas of those institutions were obvious choices. For the best coverage of the (u,v)-plane (the Fourier transform plane--see Chapter 4) using North American antennas (to simplify logistics), the third antenna should be located about one-third of the way between OVRO and NRAO. Fortunately, the 26-m (85-foot) antenna of the Harvard Radio Astronomy Station (HRAS, Fort Davis, Texas) is in almost exactly the right place. The southerly location of the HRAS dish is also advantageous for observations of low declination sources. Table 2.1 gives the coordinates of the three antennas and the resultant baselines used for processing this experiment. Also given are improved baselines determined from the data by J. Romney (private communication) using an extension of the techniques discussed by Cohen (1972).

Table 2.1

Geocentric Antenna Coordinates and the Resultant Baselines

Antenna	Radius	Latitude	Longitude
OVRO 40m	6371.600 km	37:0466	118:282
NRAO 43m	6370.792 "	38:2509	79:8363
HRAS 26m	6374.224 "	30:4678	103:947

Baseline	X	Y	Z
OVRO-NRAO	3292.392 km (3292.4728)	446.124 km (446.1398)	105.535 km
OVRO-HRAS	1085.337 km (1085.3742)	853.664 km (853.6706)	-606.585 "
NRAO-HRAS	-2207.055 km (-2207.0986)	407.540 km (407.5308)	-712.120 "

X, Y, and Z are the components of the baseline vector pointing from the first antenna to the second antenna, in a left-handed coodinate system (the X direction points towards latitude = 0°, longitude = 0°; Y towards lat = 0°, lon = 90°W; and Z towards lat = 90°N). Improved values of X and Y, determined from the data by J. Romney (private communication), are given in parentheses.

The choice of observing frequencies quickly narrowed to 5 GHz (λ = 6.0 cm) or 10.7 GHz (λ = 2.8 cm). These are standard radioastronomical frequencies for which receivers exist at many observatories. The maximum baselines would be $d/\lambda \simeq 56 \times 10^6$ at 6 cm or $d/\lambda \simeq 120 \times 10^6$ at 2.8 cm. Observations with the "Goldstack" interferometer (Cohen et al. 1971; Shaffer et al. 1972) with $d/\lambda \simeq 100 \times 10^6$ indicated that the highest possible resolution was desirable. Thus, we decided to observe at 2.8 cm, although such a wavelength puts great demands on antenna pointing and efficiency, and on local oscillator coherence properties. In addition, weather can be a severe problem, but fortunately the elements were with us for this run.

Each antenna and its associated equipment are now briefly described.

OVRO: The 40-m antenna was equipped with an uncooled parametric amplifier which gave an overall system temperature (T_s) of about 250°K. A beam-switching feed system allowed pointing and gain measurements during the experiment. The LO reference signal came from a Hewlett-Packard HP 5065A rubidium (Rb) standard. Universal Time (UT) was established by carrying a portable Rb clock to the NASA Deep Space Network station at Goldstone, California.

NRAO: The 43-m antenna had a cooled parametric amplifier and an overall $T_s \sim 100$°K. When operated in a beam-

switching mode, the system was sufficiently sensitive to allow very accurate pointing and gain measurements during the observations. The LO reference signal was provided by a modified Varian H-10 hydrogen maser oscillator. UT was established by reference to the East Coast LORAN C chain.

HRAS: The 26-m antenna used the NRAO portable 2.8 cm front end. With an uncooled parametric amplifier, the overall $T_s \sim 300°K$. The low aperture efficiency of the dish and the total power receiver required that pointing and gain curves be established prior to the experiment by looking at the strong sources Cas A, Cyg A, Ori A, and Tau A. The LO reference signal came from a Sulzer 2.5C crystal oscillator phase locked with a ∿40-sec time constant to an HP 5065A rubidium standard. (The Sulzer oscillator has superior short-term phase stability, and the Rb standard determines the long-term frequency stability.) UT was established by carrying a Rb clock to the White Sands Missile Test Center, and was checked against East Coast LORAN C.

B. The data recording system

At each station, radio source signals in the band 10708-10710 MHz were heterodyned to a 0-2 MHz video band (10710 MHz translated to DC), clipped, and sampled in the NRAO Mark II VLB recording system. (See Clark et al. 1972, Clark 1973, and Purcell 1973 for details of the Mark II

system.) The sampler takes one-bit samples (the sign of the video signal) at the Nyquist rate of 4 MHz. All frequencies in the RF conversion and sampling processes are controlled by the station reference oscillator. The samples are recorded on magnetic tape for later analysis using a modified Ampex VR-660C recorder.

C. Observing procedures

At each antenna, an observing run usually lasted for one hour, ending on the hour or when the source set at one of the antennas. At the beginning of each run, OVRO and NRAO would peak-up on the source, determine its apparent strength by doing a calibrated on-off measurement, and measure the total on-source system temperature. At HRAS, since the sources were not detectable on the strip chart record, the antenna was pointed according to previously determined curves and the on-source system temperature was measured.

D. Selection of sources

To select sources for this study, we considered the type of object, its structure, strength, and location in the sky. From previous VLB experiments, especially the Goldstack series, we had good structure information on 9 or 10 sources and indications of structure for many more

(Kellermann et al. 1971; Cohen et al. 1971; Shaffer et al. 1972).

In order to observe the hoped-for range of variation in the visibility amplitude, especially on the rather insensitive OVRO-HRAS baseline, it was necessary to pick fairly strong sources. The weakest source observed had about 7 flux units [1 flux unit (f.u.) = 10^{-26}W m^{-2} Hz^{-1}].

It is desirable to look at sources with $\delta > 0°$ in order to get long tracks in the (u,v)-plane (see Chapter 4). At $\delta = 0°$, a source has about 8 hr of common visibility between NRAO and OVRO. For $\delta \simeq 40°$, this time increases to about 11.5 hr. In addition, the (u,v)-plane is more fully sampled for higher declination sources. Figure 2.1 compares the u-v tracks for $\delta = 1°$ (representative of 3C 273 and PKS 2134+004) and $\delta = 40°$ (representative of 3C 84, NRAO 150, 4C39.25, and VRO 42.22.01). At higher declinations, the u-v tracks become more nearly circular and allow a much better measure of the source structure.

Previous experience had indicated that the best observational technique is to observe only one source at a time, rather than switch around among several sources that are nearby in the sky. Therefore, the right ascensions of the sources must be well spaced. (Several sources with similar right ascensions may be done if there are several days of observing time.) In the $2\frac{1}{2}$ days alloted for this experiment,

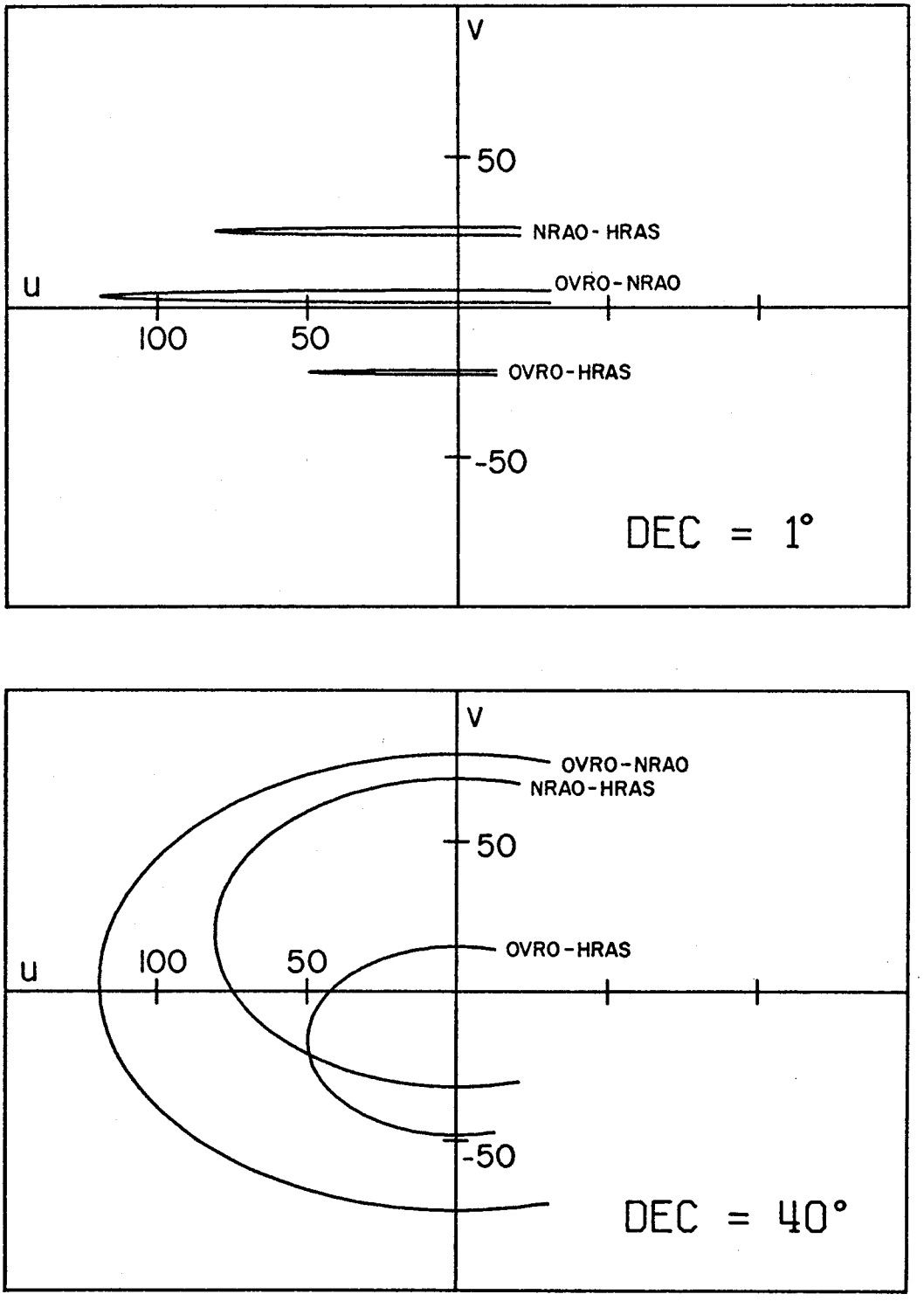

Figure 2.1 (u,v)-plane coverage for $\delta = 1°$ (upper) and $\delta = 40°$ (lower).

we could expect to do 5 or 6 sources. One of them should be a "calibrator", a source that is (hopefully!) unresolved for all baseline configurations. Both quasars and radio galaxies should be included in an effort to find any link between them.

A judicious juggling of all the desirable factors produced the sources listed in Table 2.2. They are all fairly strong and most are at high declination. Quasars, a radio galaxy, and two mysterious objects with featureless optical spectra are included.

These data were taken during the period 28 April - 1 May 1972. The observing frequency was 10708-10710 MHz. All observations were taken with linear polarization, the E-vector position angle being 0°.

Table 2.2

Parameters of the Observed Sources

Source	$\alpha(1950)$[1]	$\delta(1950)$[1]	10.7 GHz Flux Density[2]	Identi-fication[3]	z[3]
3C 84	$03^h16^m29^s.57$	+41°19'51".8	50.5 f.u.	Seyfert	0.0176
NRAO 150	03 55 45.26	+50 49 20.3	9.25	obscured	
OJ 287	08 51 57.26	+20 17 58.7	7.1	QSS?	
4C 39.25	09 23 55.33	+39 15 23.5	11.3	QSS	0.698
3C 273	12 26 33.24	+02 19 42.6	49.5	QSS	0.158
PKS 2134+004	21 34 05.23	+00 28 25.7	11.55	QSS	1.93
VRO 42.22.01	22 00 39.36	+42 02 08.6	8.05	QSS?	

[1]Positions are from Cohen (1972) and Adgie et al. (1972).

[2]Flux density at epoch of observations (1972.33) supplied by B. Andrew.

[3]See discussion of individual sources in Chapter 4 for identification and redshift references.

Chapter 3. Reduction

A. Cross-correlation processing

The first step in processing the tapes, once they have been brought to the processor at NRAO, is to find the fringes. Since the recorded signal has a 2 MHz bandwidth, the coherence time is $\sim \frac{1}{2 \text{ MHz}}$ or about 0.5 μsec. Consequently, the two tapes must be aligned in time to this accuracy. Since UT at all stations is known only to about 10 μsec, some searching is necessary to find the correct time offset. Once this has been done for two baselines (the third follows algebraically), production processing can begin.

The Mark II correlator and associated computer programs are described by Clark et al. (1972), Clark (1973), and Purcell (1973). The correlator takes the two bit streams from the video tapes, corrects them for geometrical time delay and clock errors, multiplies them together (after removing the natural fringe rate) and integrates the results for 0.2 sec. The output from this process is the cross-correlation function, which represents the fraction of the noise power at the two antennas which is correlated. This is done for 31 different delays, separated by 1/4 μsec, centered on the expected time delay.

The 0.2 sec records are then analyzed by looking for a sinusoidal component in the cross-correlation function.

This component is called the "fringes". For the detection of weak signals and to minimize the effects of noise, it is desirable to integrate the fringes coherently for as long as possible. The integration time is usually limited by the eventual loss of coherence between the two local oscillators. For hydrogen masers, the coherence time at 2.8 cm is many minutes. For rubidium standards, the time is 20-30 seconds, improving to 1-2 minutes for the phase-locked Sulzer system. The results of an integration are the amplitude and phase of the fringes in the cross-correlation function. I have used only the amplitudes for model fitting (see Chapter 4) since the phases are almost arbitrary due to oscillator instabilities and frequency errors, atmospheric effects, and baseline and source position errors.

The data presented here have been coherently integrated for 15 seconds and incoherently averaged for 8 minutes (except for shorter intervals when there is a break in the data, and 4 minutes for that part of the 3C 84 data where the correlated flux density is varying rapidly with time: $0<IHA_{O-N}<2$ in Figure 4.2a).

B. Calibration

After correlating the data, one has a great mass of numbers that need calibration. This term is used to denote the process that turns correlation coefficient amplitudes

into flux units, the radio astronomers' standard.

With the one-bit system used for these data, the cross-correlation coefficient between antennas 1 and 2 (ρ_{12}) is related to the one-bit correlation coefficient ρ by $\rho = \frac{2}{\pi} \sin^{-1} \rho_{12}$ (Van Vleck and Middleton 1966).

Since $\rho_{12} << 1$ (0.001 is typical),

$$\rho = \frac{2}{\pi} \rho_{12} . \tag{3.1}$$

For system temperatures T_i and antenna temperatures T_{A_i} at antennas 1 and 2,

$$\rho_{12} = \gamma \sqrt{\frac{T_{A_i}}{T_1} \frac{T_{A_i}}{T_2}} \tag{3.2}$$

where γ is the unknown source visibility amplitude (Cohen 1973). Conversely, since $T_{A_i} = \frac{S \eta_i A_i}{2k}$ (for an unpolarized source), where S is the source flux density, η_i is the aperture efficiency, A_i is the antenna area, and k is Boltzmann's constant, we get a measure of the correlated flux density

$$S_c = \gamma S = b \rho_{12} \sqrt{\frac{T_1 T_2}{\eta_1 \eta_2}} \frac{2k}{\sqrt{A_1 A_2}} \tag{3.3}$$

for each value of ρ_{12}, where b is a scale factor.

Theoretically, since the T_i's and η_i's are known from measurements during the observations, equation (3.3) should be sufficient to calibrate the correlated flux density scale. In practice, S_c calculated from equation (3.3) is always too low by a factor of 2 or so because of various instabilities and computing techniques, and the experiment is calibrated

by observing a source that is assumed (hoped!) to be unresolved ($\gamma = 1$). For such a source, the correlated flux density equals the total flux density, and the scaling factor b can be determined. For this experiment, we observed OJ 287 as the calibrating source. Previous data (Cohen et al. 1971) indicated that OJ 287 should be essentially unresolved at our maximum baseline of 120×10^6 λ. The source was observed 6 times over a wide range of hour angles and did indeed seem unresolved (see Figure 4.7a).

For estimated aperture efficiencies of 0.4, 0.4, and 0.2 (OVRO, NRAO, HRAS) and the system temperatures given in Chapter 2, the values of b for OJ 287 are 2.39, 2.49, and 2.11 (reduced by 10% to 1.90, see the next paragraph) for the OVRO-NRAO, OVRO-HRAS, and NRAO-HRAS baselines respectively. These values of b were not actually used, however. Instead, scale factors requiring only relative (rather than absolute) values of T_i and η_i were determined.

A constraint on the scaling is that no source can have a visibility greater than unity at any hour angle. The original scaling for the NRAO-HRAS baseline resulted in $\sim$10% excess correlated flux density for 3 sources. The reason for the excess is unknown. Perhaps all the errors conspired in the same direction (see the next section). I have rescaled this baseline down by 10%. An additional check on the NRAO-HRAS scaling comes from the crossing of the OVRO-HRAS and

NRAO-HRAS tracks in the (u,v)-plane for 3C 84 (see Figure 4.2b). At that point, the correlated flux density must be the same for both baselines. The rescaled NRAO-HRAS results agree with the OVRO-HRAS results to better than 4%.

From the above consideration, it seems that these data have been calibrated relatively to better than 5% from baseline to baseline, although the overall calibration could be systematically in error. It seems highly unlikely that the scale factors could be too small by more than 5%, and unlikely from other experiments that they could be too large by more than 10% (Cohen et al. 1971; Shaffer et al. 1972; Clark et al. 1973).

C. Errors

The accuracy of the scaling discussed above and the goodness of fit of the models presented in Chapter 4 depend on the errors of the individual data points. Such errors come from three different sources: system noise temperature, antenna gain and noise temperature calibration, and effects due to the nature of the experiment (equipment, atmosphere, processor, etc.).

System noise temperature: All radio astronomical observations are limited in sensitivity by the noise characteristics of receivers and signals. As derived in the Appendix, consideration of our one-bit system and the scaling fac-

tors for the three baselines gives values of the observed rms noise (σ_s) for one 15-second integration of ∿0.43 f.u., ∿1.0 f.u., and ∿1.7 f.u. for the OVRO-NRAO, NRAO-HRAS, and OVRO-HRAS baselines respectively.

We can also calculate directly the expected rms fluctuations by using equations (3.1), (3.3), and $\sigma_\rho = \frac{1}{\sqrt{N}}$ (Purcell 1973), where N is the number of one-bit samples used to determine ρ. Setting $\rho = \sigma_\rho$, the expected rms correlated flux density error is

$$\sigma_s = b\frac{k}{r_1 r_2}\frac{1}{\sqrt{N}}\sqrt{\frac{T_1 T_2}{\eta_1 \eta_2}} \quad , \qquad (3.4)$$

where r_i is the radius of antenna i. For Nyquist sampling, N = 2Bt for bandwidth B and integration time t. Equation (3.4) with the values of b, T, and η mentioned earlier, gives σ_s's slightly smaller than those in the preceding paragraph. This is because the Appendix used typical rather than optimum values of T and η to determine σ_s.

Antenna gain and system temperature calibration: We must know the parameters in equation (3.3) to correct each value of ρ_{12}. This means measuring the system temperature for each run and measuring the source antenna temperature run-by-run or knowing the antenna gain as a function of position and assuming the antenna is pointed correctly. None of these quantities need be known absolutely, since they will be accounted for in the final scaling. Table 3.1 gives the

relative accuracy to which these parameters are believed to be known.

Table 3.1

Relative accuracy of System Temperature and Antenna Gain

Station	T_s Error	T_A or Gain Error
OVRO	3%	5%
NRAO	1%	3%
HRAS	2%	5%

The square root in equation (3.3) will approximately halve each of these errors and they will add in quadrature to give the estimated system calibration accuracy for each baseline. Table 3.2 presents the results. Except for the strong sources 3C 84 and 3C 273, these errors are comparable to those from noise effects.

Table 3.2

Overall System Calibration Accuracy

Baseline	System Calibration Error
OVRO-NRAO	3.3%
NRAO-HRAS	3.1%
OVRO-HRAS	4.0%

Examination of the raw correlation coefficients indicates that the estimates in Table 3.1 for antenna gain errors are rather optimistic. There are occasional correlated

trends in the data from two baselines as would occur if the common antenna were drifting off the source, as it might well do during an hour-long run. Fortunately, such effects are usually small. There are two or three occurences of gross pointing errors. Those data have been eliminated from all model fitting and the graphs in Chapter 4. It is clear that higher accuracy experiments will require better knowledge of the system temperatures and antenna gains.

Equipment and other effects: The Mark II recording and reduction process may add some errors. Since it is digital in nature, there are some analog functions that it must approximate, such as stepping time delays and offsetting fringe rates. Although they reduce the sensitivity slightly, these effects should average out and be taken care of by the scaling. There are occurences of apparent misalignment of the playback units which give incorrect correlation coefficients. I believe all such occurences have been detected and reprocessed or eliminated.

The algorithm that finds correlation coefficient amplitudes is systematically biased towards overestimation, especially for data with low signal-to-noise ratio (Purcell 1973). See the Appendix for further discussion and my method for treating weak signals.

Phase instabilities due to local oscillators, multiplier chains, the atmosphere, and any other sources will conspire

to reduce the cross-correlation coefficients. The instabilities will be different for each baseline, but the overall scaling should remove the differential effects. Again, the average result should be only a reduction in sensitivity. There are occasional data that seem excessively high or low. They may be due to brief periods of exceptional phase stability or instability, or intermittent equipment malfunctions.

An overall estimate of the errors for each datum has been made by adding in quadrature the errors from noise ($\sim$0.43 f.u., $\sim$1.0 f.u., and $\sim$1.7 f.u. for the OVRO-NRAO, NRAO-HRAS, and OVRO-HRAS baselines respectively) and a 5% calibration error. Noise errors have been reduced by the square root of the integration time in excess of the 15-second interval that gives the above rms values. Confidence in the relative scaling between the baselines is boosted by the goodness of fits described in Chapter 4. All fits were made after the baseline scaling, and it seems unlikely that gross scale errors would be compatible with the simple models that result.

Chapter 4. Results

A. Introduction

Consideration of the geometry of an interferometer and the multiplying correlation process leads to the following expression for the output from the correlator:

$$\mathcal{V}(u,v) = Ve^{i\Phi} = K\iint T_b(\alpha,\delta)\ e^{2\pi i(\alpha u+\delta v)}\ d\alpha d\delta\ . \qquad (4.1)$$

$\mathcal{V}(u,v)$ is usually called the complex visibility function and is the Fourier transform of $T_b(\alpha,\delta)$, the radio source brightness distribution (Moffet 1961). u and v are the East-West and North-South projections of the baseline (in wavelengths) onto the plane of the sky. K is a scale factor. If a pair of antennas track a particular point in the sky for an extended length of time, u and v trace out part of an ellipse in the Fourier transform plane, usually called the (u,v)-plane for brevity. If B_1 is the equatorial projection of the baseline, B_2 the North-South component of the baseline (B_i in wavelengths), and δ the declination of the source being studied, the ellipse has major axis B_1, axial ratio sin δ, and is centered on u=0, v=B_2 cosδ.

Ideally, with a sufficient number of measurements, equation (4.1) could be inverted to give $T_b(\alpha,\delta)$. However, in VLB practice, all we are able to measure is the modulus V of the visibility function. Also, our coverage of the

(u,v)-plane is limited by the availability of antennas and the less-than-24 hour coverage possible for most sources.

Therefore, to interpret the data gathered for this thesis, I have resorted to model fitting techniques. From an examination of the visibility curves for the three baselines and the appropriate u-v tracks, one can usually make a guess (or several) at the most obvious details of the brightness distribution of a source. Then the guess is given to the least-squares fitting program discussed by Purcell (1973). That program gives the best estimates of the parameters of the assumed model (subject to restraints on the variation of highly-correlated parameters).

For most sources, I have tried several models since my limited u-v coverage usually doesn't indicate a unique model. My model guesses are greatly prejudiced by the structure observed for much more extended sources. See Macdonald et al. (1968) for typical structure maps. Nevertheless, it is remarkable how well simple doubles and elliptical Gaussians fit the data in many cases.

I emphasize that all models presented here agree with the data from all three baselines. Previous work from single baselines often produced models that fit the data very well, but the incomplete u-v coverage left nagging doubts about their validity. These new data have very good

coverage (especially for $\delta \simeq 40°$) and inspire a good deal of confidence in the models. With a (u,v)-plane cell size of about $40 \times 10^6 \lambda$ and a maximum baseline of $120 \times 10^6 \lambda$, this experiment is sensitive to all angular scales between 0".005 0".0005. Although ambiguities remain in the models, it is unlikely that we have missed any structure information on these scales.

Figure 4.1 illustrates the reason for some of the ambiguities in the models. The figure shows the ratio of visibility amplitudes for a Gaussian, a disk, and a double brightness distribution whose sizes have been chosen to have the same half-power transform width. It is obvious that we must observe visibilities $\lesssim 0.4$ in order to distinguish among the various possible brightness distributions. Since my data seldom go that low, I have used only elliptical Gaussian components for all my models.

Sometimes a model will quote a "point" component. Such a result refers to a component $<0".0003$ in diameter. That size corresponds to $\gamma > 0.90$ at my highest resolution. The brightness temperature limit set by inverse Compton scattering gives a comparable size (Kellermann and Pauliny-Toth 1969).

I cannot emphasize too strongly that the models presented here are just that -- models. Although the models fit the observed data, we have surely overlooked complex

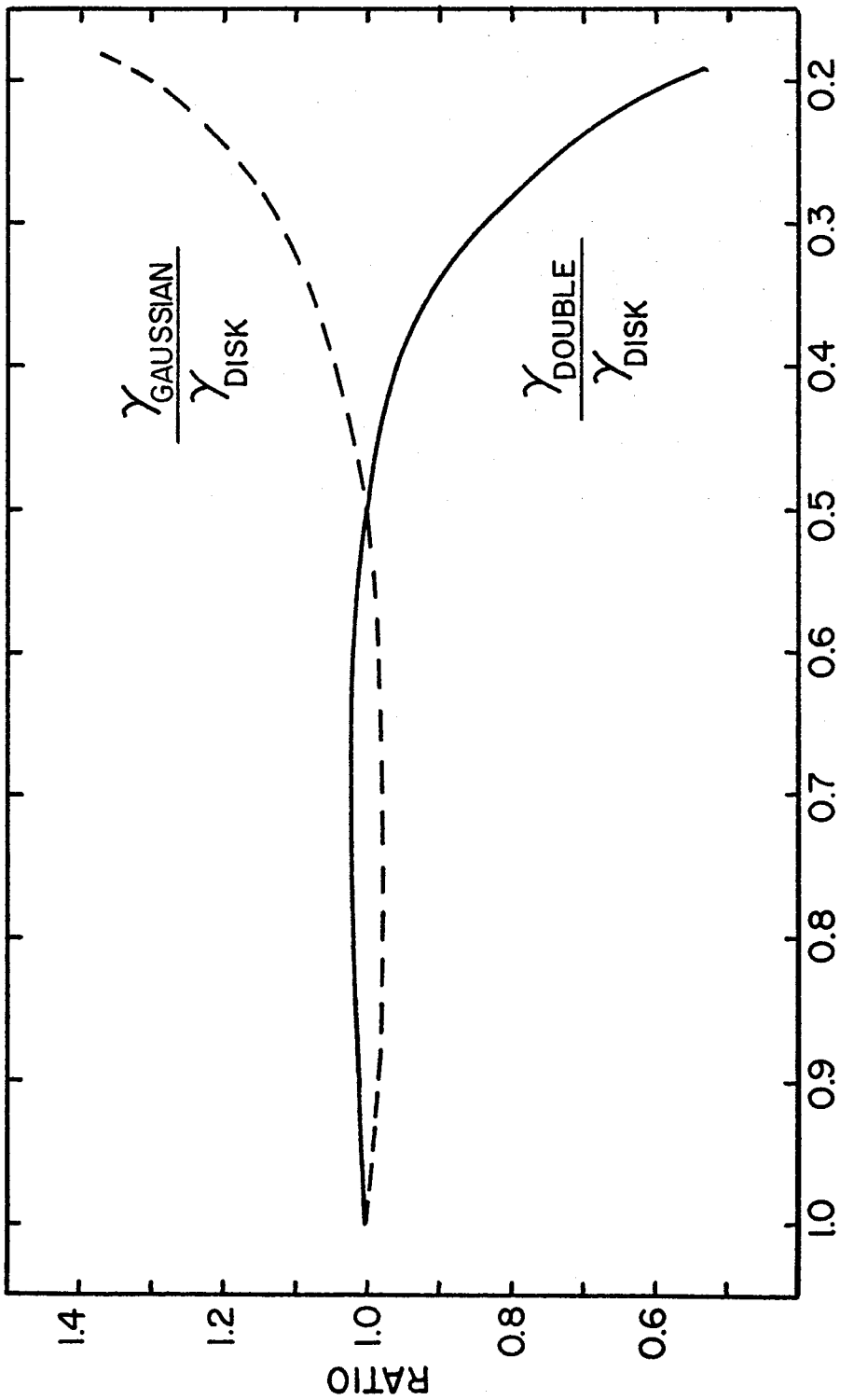

Figure 4.1 Ratio of visibility amplitudes for a Gaussian, a uniform disk, and an equal point double brightness distribution, as a function of the spacing that produces a given resolution of the disk ("Normalized visibility"). The three brightness distributions have sizes which give the same half-power transform width.

details of the source brightness distributions. However, the crude details of the overall structure must be more or less as given. As the reader bears in mind these caveats, I will describe each of the observed sources.

For each object, the three visibility curves, a plot of the (u,v)-plane coverage, and the spectrum are given. In some cases, a suggested decomposition of the spectrum into several separate components is also shown. This break-up assumes that there are several distinct regions of the source. It is these regions that correspond to the several components that comprise a model source distribution. A source radiating by the synchrotron mechanism will show the effects of self-absorption if it is sufficiently small and luminous. Such synchrotron self-absorbed objects are believed to comprise the sources under study. See Kellermann and Pauliny-Toth (1969) for a discussion of compact sources and Terrell (1966) for a derivation of their expected spectrum.

I have used VLB and other data from a wide range of frequencies in an attempt to define individual self-absorbed components. In some cases, it seems possible to show directly the $S_\nu \propto \nu^{2.5}$ behavior expected for the optically thick part of a synchrotron self-absorption spectrum. The compact components should show sharp edges at frequencies below their spectral peaks, and probably have less distinct

boundaries at higher frequencies. As mentioned earlier, the present data cannot distinguish such appearances, but efforts should be made to look for these differences.

From peak flux density, frequency of the peak, and the angular size of these components, we can calculate the magnetic field in the compact sources. This is done in Chapter 5.

B. Guide to the figures

For each source there is a plot of the visibility data, the u-v tracks, and the spectrum.

Visibility data: Each plot gives correlated flux density in flux units as a function of interferometer hour angle (IHA). IHA is the best parameter for the time axis since it allows easy comparison between data from various experiments. The data bars represent ±1 standard deviation as calculated in Chapter 3. The baselines are OVRO-NRAO, NRAO-HRAS, and OVRO-HRAS from top to bottom. Solid lines through the data are the predicted visibilities for models discussed in the text. S_T is the total 10.7 GHz flux density at the epoch of the observations (kindly supplied by B. Andrew).

u-v tracks: The given tracks represent the actual coverage for this experiment. The arrow heads point in the direction of increasing time. The scales are in millions of

wavelengths. The maximum value of u (u_{max}) occurs at IHA = 0. U_{max} is 120, 80, and $50 \times 10^6 \lambda$ for the OVRO-NRAO, NRAO-HRAS, and OVRO-HRAS baselines respectively.

Spectrum: The flux density spectrum is given at the approximate epoch of observation. All the sources are variable and some interpolation from published data is necessary. The abcissa is in megahertz and the ordinate in flux units.

Individual components suggested by my data and other interferometry results have been drawn in for some sources. The components are labelled with capital or small letters alphabetically in order of increasing peak frequency. The letter designations are not intended to correspond to any previous nomenclature. For several sources, additional interferometric data at various frequencies are plotted and identified in the individual captions.

Spectral data are taken from Artyukh et al. (1969), Berge and Seielstad (1972), Dent and Hobbs (1973), Dent and Kojoian (1972), Erickson and Cronyn (1965), Kellermann et al. (1969), Kellermann and Pauliny-Toth (1971), Kraus and Andrew (1970), Medd et al. (1972), Shimmins et al. (1968), and private communications from B. Andrew, W. Dent, and R. Ekers.

3C 84

3C 84 (NGC 1275) is one of the original Seyfert (1943) galaxies. The redshift is 0.0176, measured by Humason et al. (1956). Optically, the galaxy shows evidence of violent activity (Minkowski 1957; Lynds 1970) which may be related to the compact radio source, although Lynds describes H_α filaments that reach $\sim$70 kpc from the nucleus.

The radio structure of 3C 84, both the compact and extended emission, is the most complex of any of the sources in the present discussion. Indeed, no believable model could be found to match the VLB observations. The visibility data given in Figure 4.2a may be qualitatively understood as coming from a double source with elongated components and probably a third (or several) more extended component. The double structure has separation $\sim$0".005 in position angle (PA) -10°. The lower maximum at $IHA_{O-N} = -1^h.5$[1] indicates that the double components are elongated approximately along the direction of separation. The high correlated flux density at $IHA_{O-N} = +1$ implies a width $\lesssim$0".0009 for the most compact structure, perpendicular to the double orientation. The large visibility at $IHA_{O-H} = +3$ indicates that $\gtrsim$0.85 of the source is in components $\lesssim$0".002 in length in PA 80°.

---

[1] I will use subscripts O-N, N-H, and O-H to denote baselines.

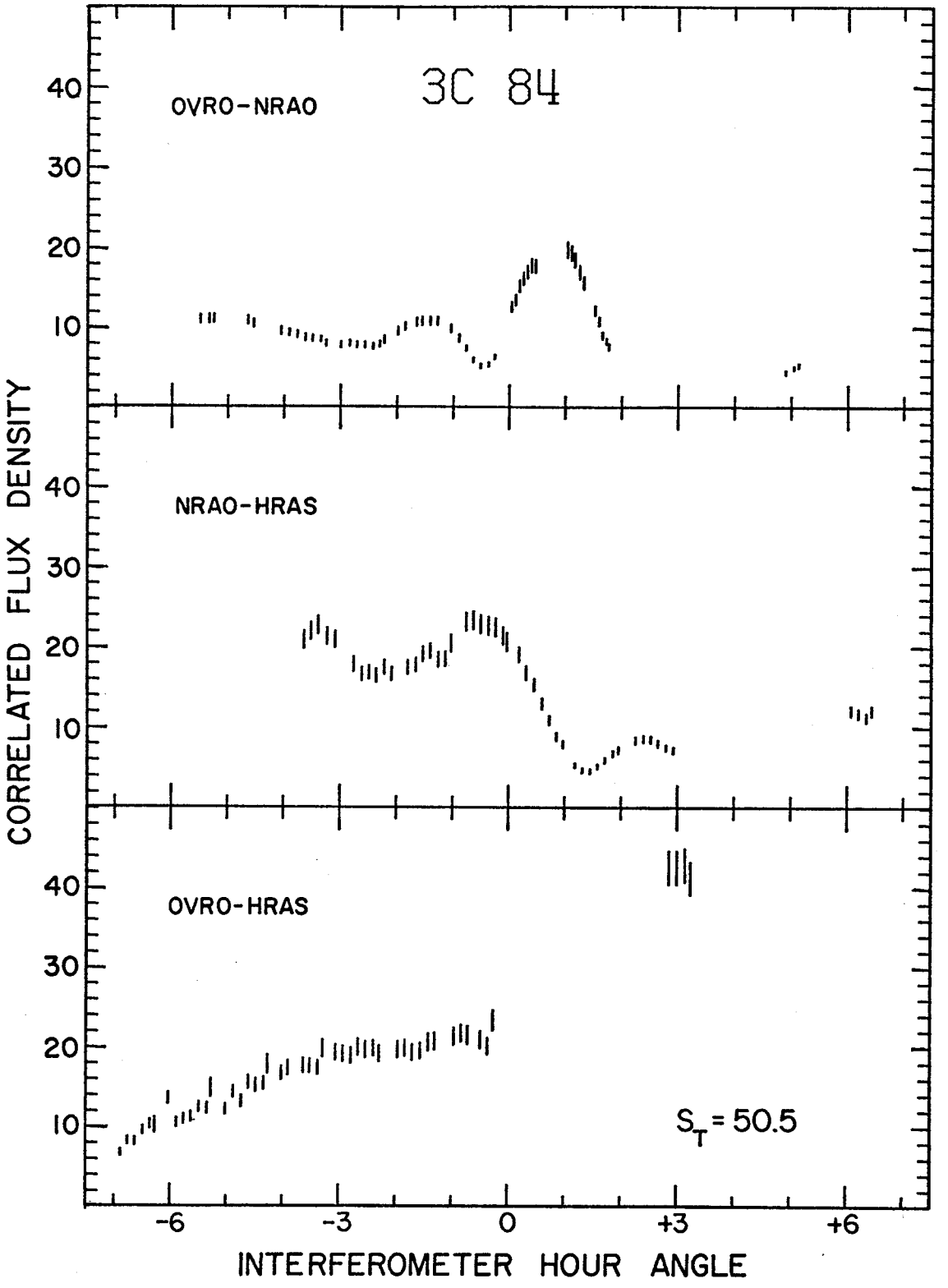

Figure 4.2a The visibility data for 3C 84. See p. 28 for additional description.

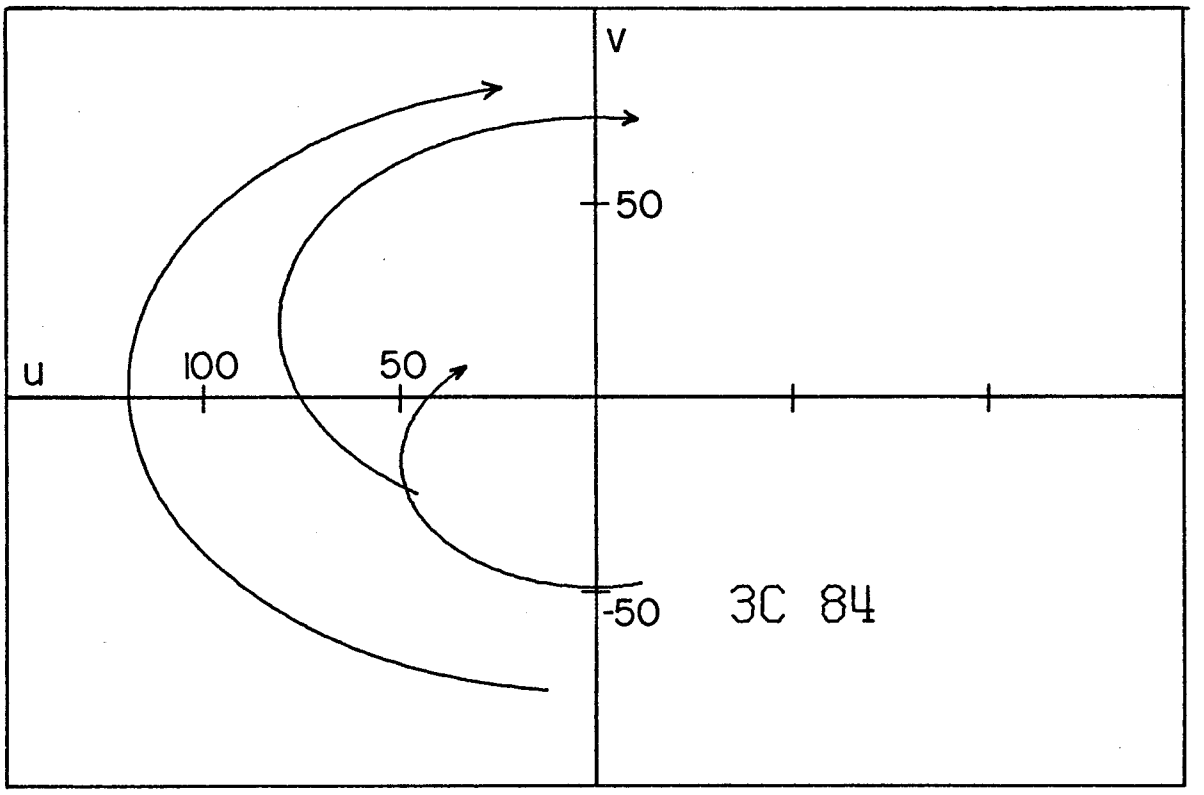

Figure 4.2b The u-v coverage for 3C 84. See p. 28 for additional description.

The spectrum of 3C 84 is given in Figure 4.2c along with a partial decomposition. Interpretation of older interferometric data is complicated by the time variation of the flux density, presumably of the compact components. Nevertheless, we can make some likely suggestions.

The most extended radio structure associated with 3C 84 itself is a halo of several arc-minutes in extent (Ryle and Windram 1968). The spectrum of the halo is well defined by low frequency total flux measurements and 75, 21, 11, and 6 cm long baseline data (Wilkinson 1972; Donaldson et al. 1969). The spectral index of the halo is rather steep, $\alpha = -1.14$ where $S_\nu \propto \nu^\alpha$, but not unusual. The halo is component A in Figure 4.2c.

Moderate resolution data at 75, 67, 50, and 18 cm (Clarke et al. 1969; Purcell 1973; Kellermann et al. 1971) as well as the interferometry mentioned just above provide good evidence for a component (or components) of size $\sim$0".025 whose spectrum peaks at about 8 f.u. at 500 MHz (component B in Figure 4.2c). Higher resolution 18 and 13 cm observations (Kellermann et al. 1971; Broderick et al. 1972) completely resolve the 0".025 component and appear to refer to the optically thick, low frequency side of the components observed at 2.8 cm.

The three (or more) high frequency components referred to above have not been drawn in Figure 4.2c because there is

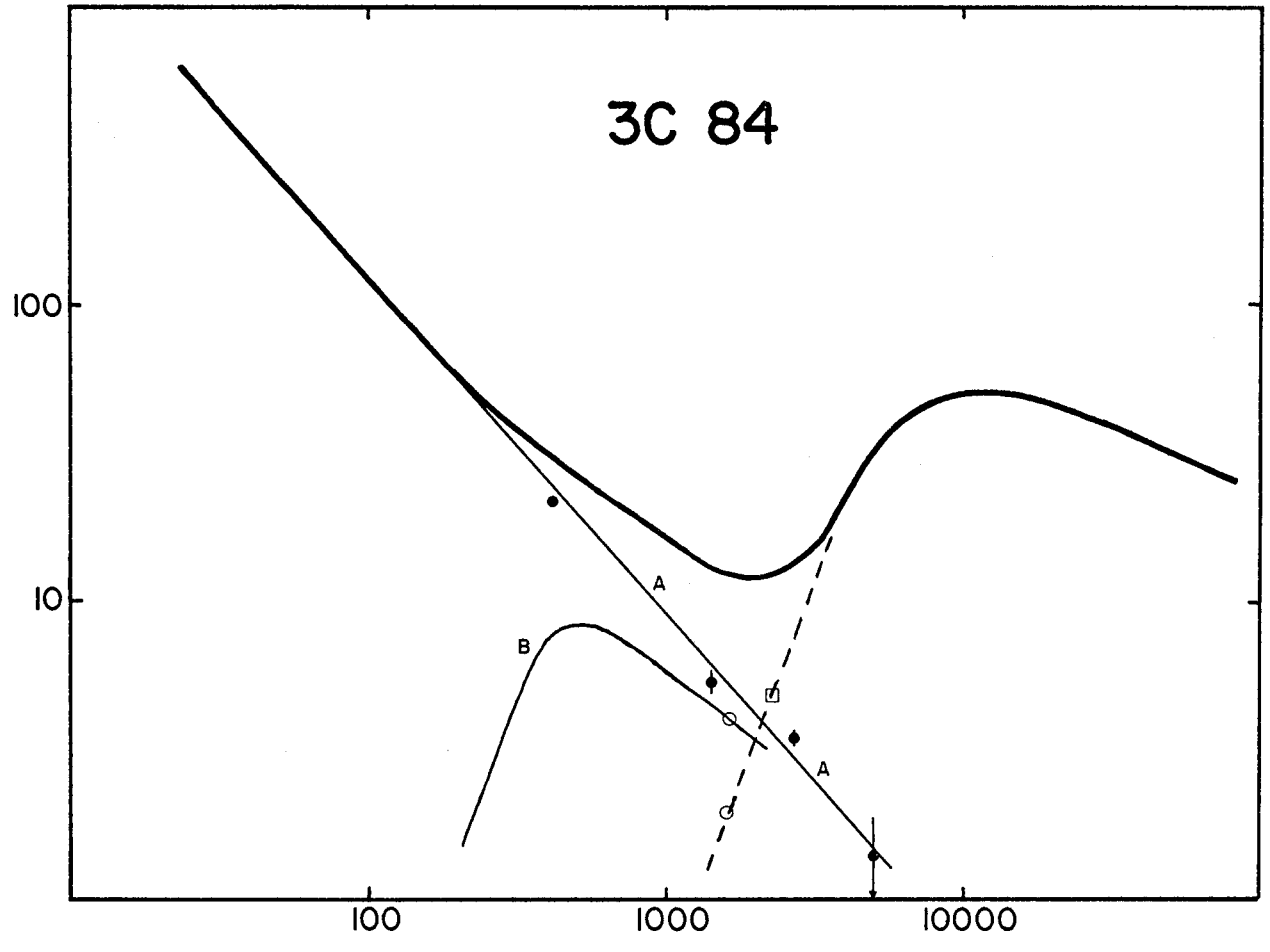

Figure 4.2c The spectrum of 3C 84, with a partial decomposition into several components. See p. 29 for additional description.

- ♦ Flux in extended component from Donaldson et al. (1969) and Wilkinson (1972).
- ○ 18 cm measurements of Kellermann et al. (1971).
- □ 13 cm measurements of Broderick et al. (1972).

not enough information to identify them uniquely. I suspect the more extended component contributes most of the flux below 8 or 10 GHz and the two components that make the double source peak at frequencies near or above 10 GHz. Observations at 3.8 cm (Cohen et al. 1971; Shaffer et al. 1972), these data and further observations at 2.8 cm by our group and Legg et al. (1973), and unpublished results at 2 cm are all roughly consistent with the 0".005 separation and PA -10° double structure, although the details aren't understood. The 3.8 cm data are too sparse (and the 2 cm data so far uncalibrated) to give good information about the spectrum of the most compact parts of the source.

Legg et al. (1973) (whose flux scale appears to be a factor of $\sim$3 too low) model their single baseline data with 4 components, a seemingly optimistic result. Their point model is ruled out by these data, and their extended component model fits my data very poorly, although Yen (private communication) reports that it can be modified to fit my data. Without more complete information from more baselines and other frequencies, it seems premature to decide the compact structure of 3C 84 at this time.

NRAO 150

The galactic latitude of NRAO 150 is -2°, and the source is obscured and unidentified.

The visibility curves for the three baselines and the appropriate u-v tracks are shown in Figures 4.3a,b. Two simple models fit the data exceedingly well. The simplest is a Gaussian ellipse 0".00076 x 0".00015, with the major axis in PA 60°, containing all the flux (this is component b in Figure 4.3c). The major axis (±0".00003) and position angle (±5°) are well-determined, but the axial ratio is poorly known (± a factor of 2)[2]. χ^2 per degree of freedom[3] is 0.68 for the ellipse. An equal point double model (components B and C in Figure 4.3c) with separation 0".00060 ± 0".00002 in PA 59° ± 4°, also containing all the flux, has a χ^2 of 0.71. The predicted visibility curve for the double is given by the solid line in Figure 4.3c. The ellipse model predicts virtually the same line. Other models, such as elliptical disks and unequal doubles, would give comparably good fits. Higher resolution is required to decide among these possibilities.

---

[2]The given errors are those that increase the rms residuals from the best fit by 10%, while varying only that parameter. The errors refer only to the goodness of fit of the model, not its validity!

[3]All models have been fit to 100 points (except for VRO 42.22.01 which had only 67 points available) selected from the available data. From 3 to ∿10 parameters have been determined for the models, leaving ∿95 degrees of freedom.

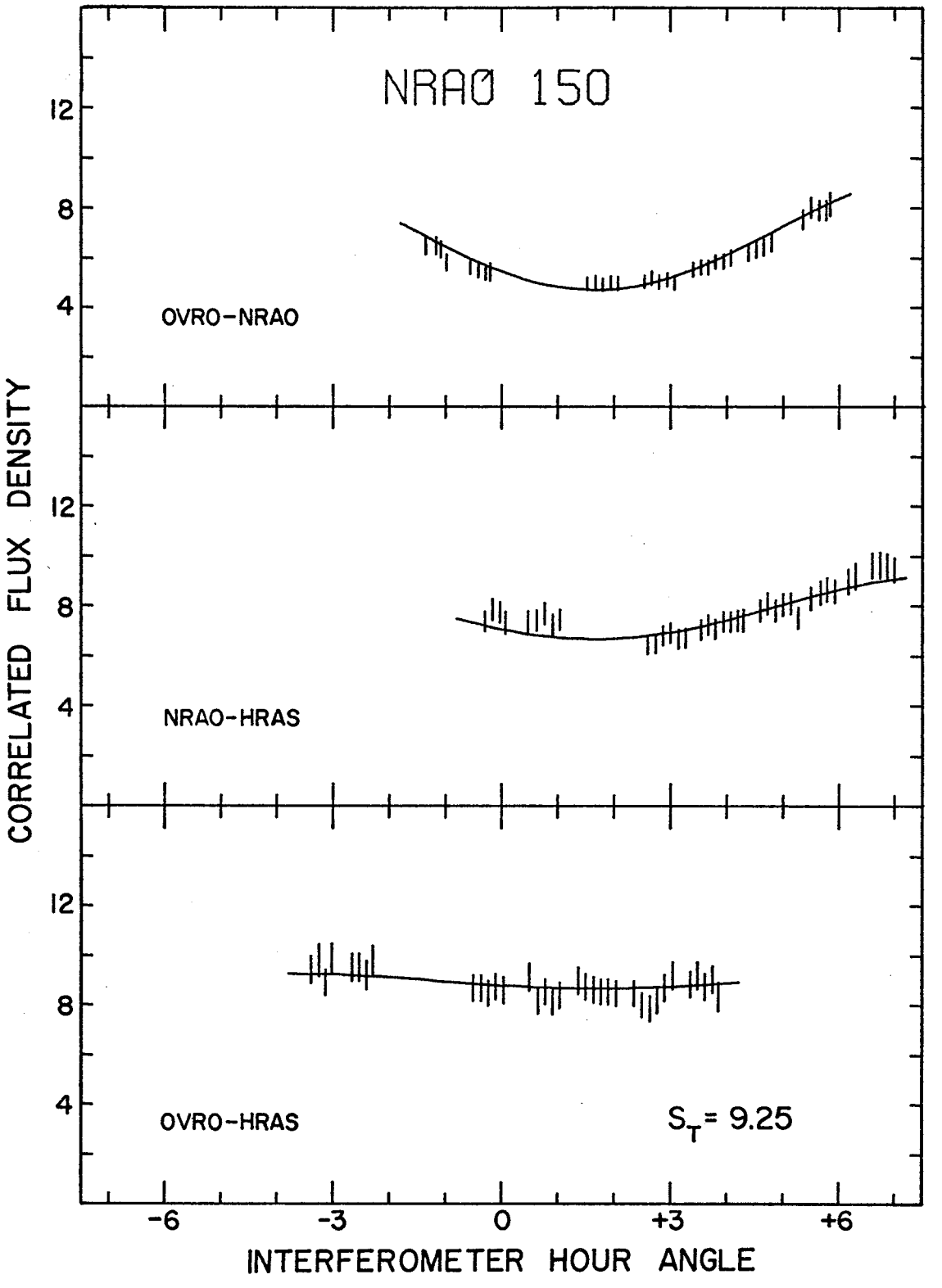

Figure 4.3a The visibility data for NRAO 150. The solid line is the predicted visibility for the point double discussed in the text. See p. 28 for additional description.

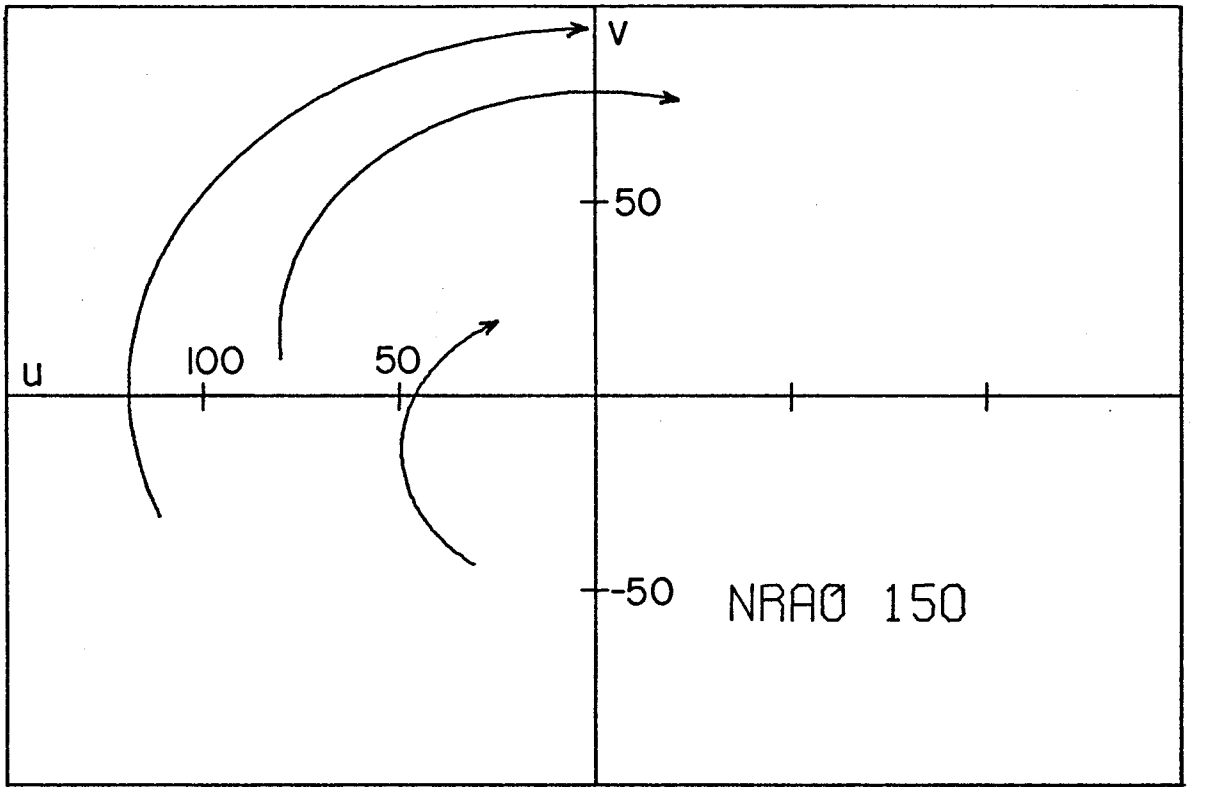

Figure 4.3b The u-v coverage for NRAO 150. See p. 28 for additional description.

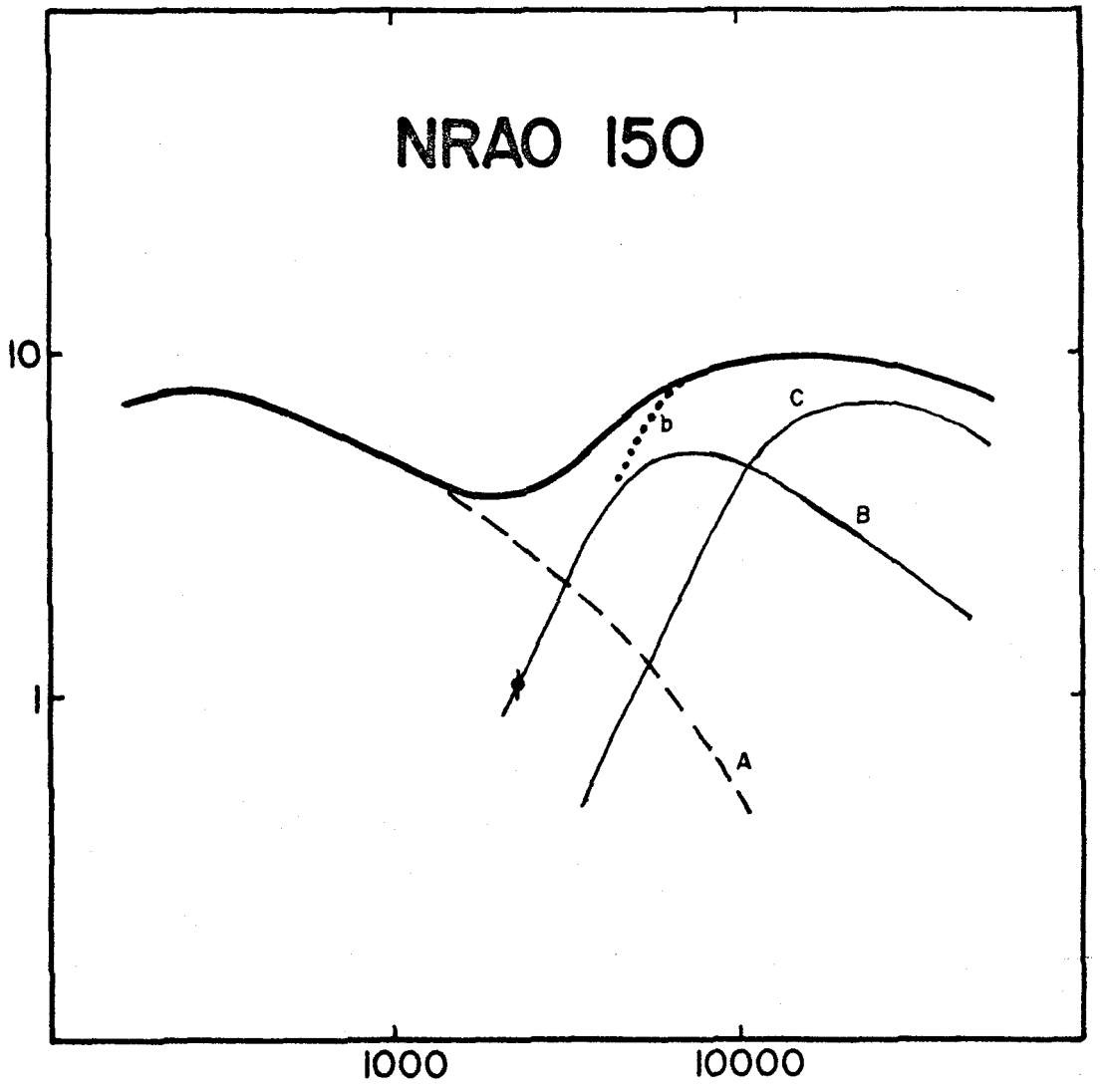

Figure 4.3c The spectrum of NRAO 150, with two possible decompositions into components. See p. 29 for additional description.

♦ 13 cm measurement of Broderick et al. (1973)

(See Figure 4.1. An increase in baseline length of less than 25% would probably give $\gamma < 0.4$.)

Figure 4.3c gives the spectrum of NRAO 150 and two suggested high frequency decompositions. A single 18 cm measurement (Kellermann et al. 1971) indicates a low frequency component of size less than $\sim$0".014, with unknown structure. This is component A in Figure 4.3c. At 13 cm, Broderick et al. (1973) resolve component A and see 1.1 f.u. from an unresolved ($\theta \lesssim$ 0".002) source. At 6 cm, approximately 0.7 of the source is in the high frequency component(s) (components B and C, or b) (Kellermann et al. 1971). The 6 cm data are quite sparse, but they are roughly consistent with the present results, although the apparent size of the source might have been greater. 3.8 cm data (Cohen et al. 1971; Shaffer et al. 1972) are in very good agreement with the 2.8 cm data, with 0.9 of the 3.8 cm flux density coming from the smallest component(s).

I prefer the double model for NRAO 150 because it is then more similar to the other sources in this experiment. Chapter 5 discusses this topic further.

4C 39.25

4C 39.25 is a 17th magnitude quasar with a redshift of 0.698 (Lynds et al. 1966). Figures 4.4a,b give the visibility data and u-v tracks.

This source has the best-determined, least ambiguous structure at 2.8 cm of any source in this experiment. The several u-v tracks cross both maxima and a minima of the brightness transform. The resulting model is an unequal double with slightly resolved components. The double separation is 0".0020 ± 0".0001 in position angle 98° ± 3°. The two components contain all the flux and have an intensity ratio of ∿4.5:1. The stronger component has a Gaussian width of ∿0".0004 and the weaker, ∿0".0006. These sizes are poorly determined, especially for the weaker component. (The Gaussians were constrained to be circular.) χ^2 per degree of freedom is 1.00 for this model, which is drawn as a solid line in Figure 4.4a.

Despite the goodness of fit to the present data, the overall structure of 4C 39.25 isn't so clear. Two possible breakdowns of the spectrum are given in Figure 4.4c. Time variations of the total flux density make interpretation of earlier VLB work somewhat hazardous; but undeterred, I make the following suggestions.

There appears to be a low frequency halo (component A of

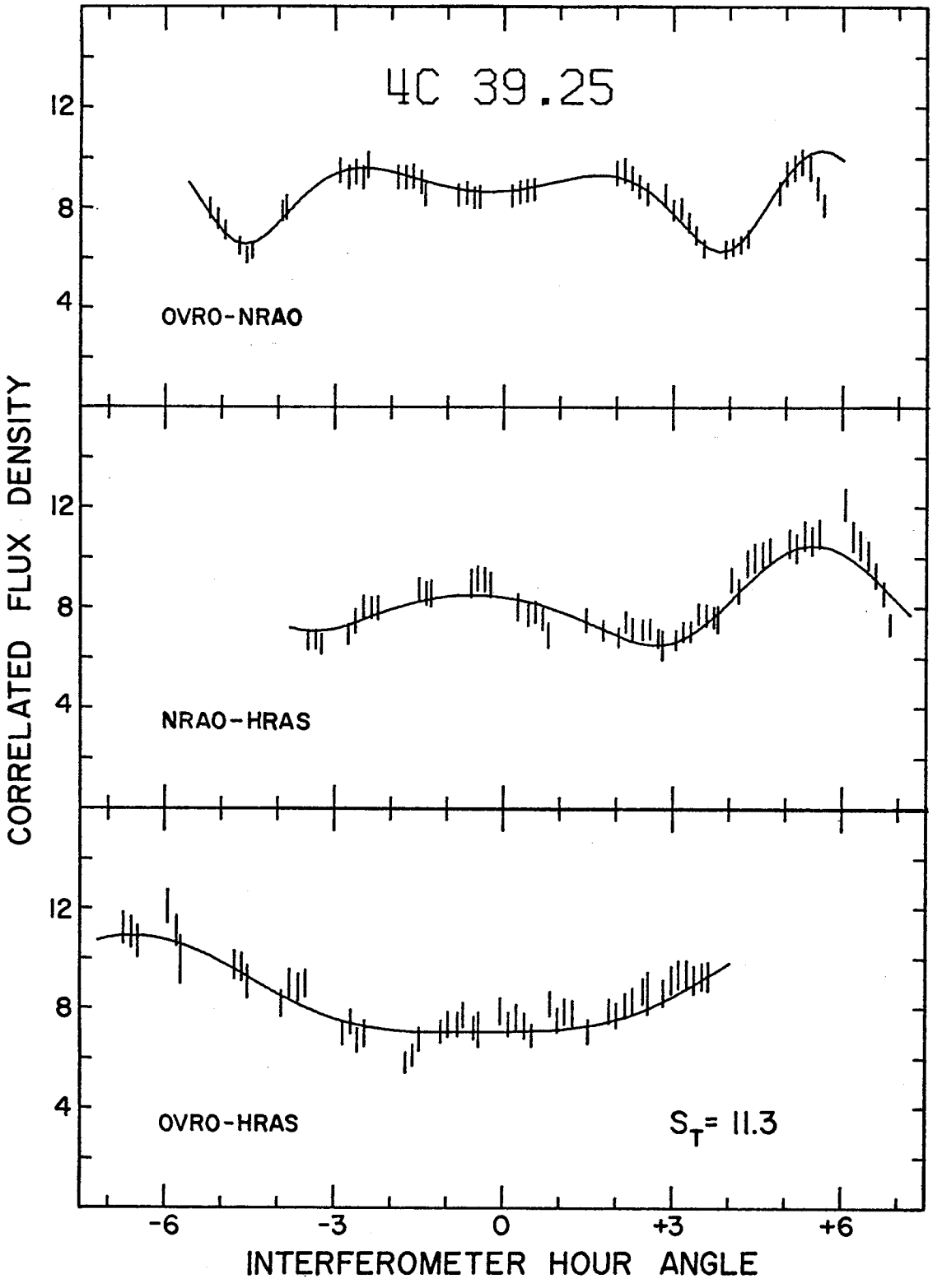

Figure 4.4a The visibility data for 4C 39.25. The solid line is the predicted visibility for the unequal double model discussed in the text. See p. 28 for additional description.

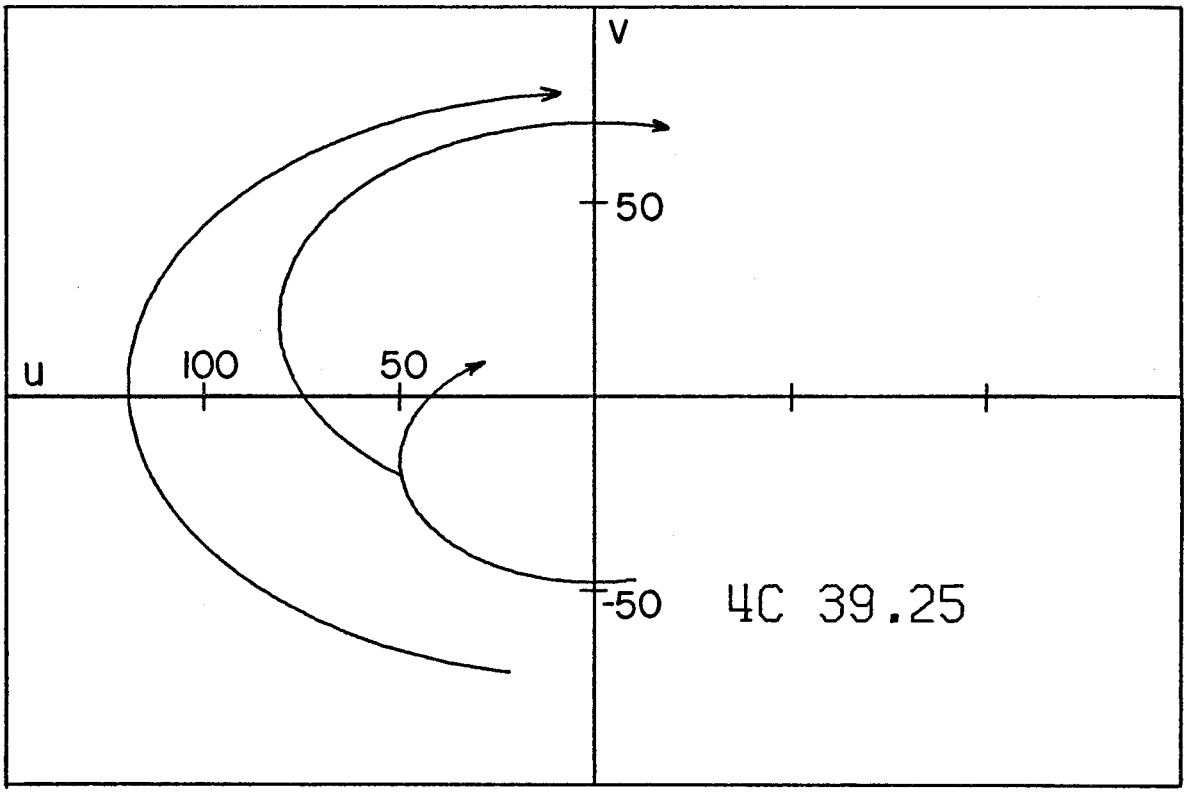

Figure 4.4b The u-v coverage for 4C 39.25. See p. 28 for additional description.

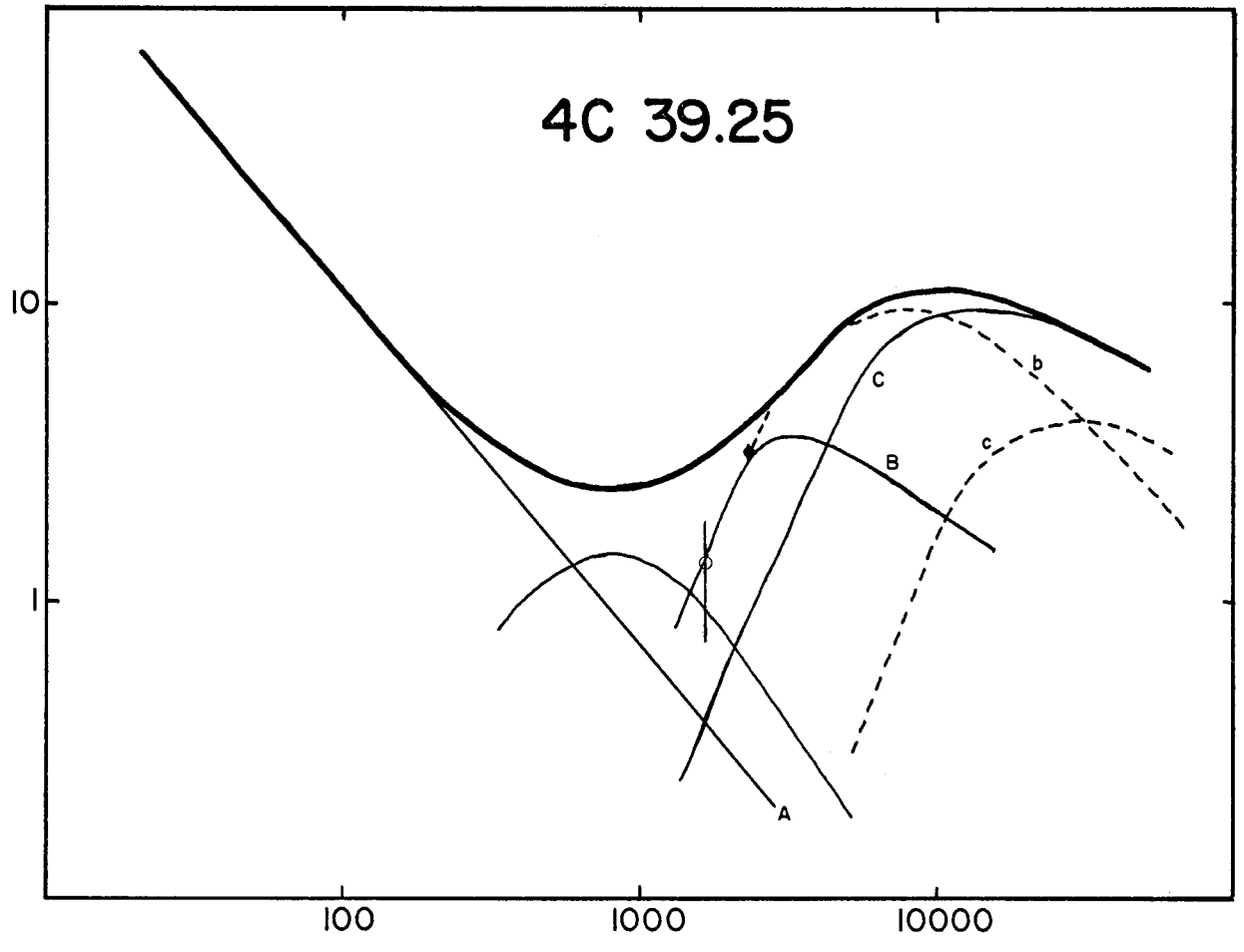

Figure 4.4c The spectrum of 4C 39.25, with two possible decompositions into components. See p. 29 for additional description.

ϕ 18 cm measurements of Kellermann et al. (1971).

$\blacklozenge$ 13 cm measurements of Broderick et al. (1972).

Figure 4.4c) of unknown extent that provides most of the flux below ∿200 MHz. There may also be a compact component whose spectrum peaks around 1 GHz. Low frequency, low resolution VLB should be able to provide evidence for or against the existence of such a component.

At 18 cm, there is ∿1.4 f.u. from components ≲0".004 (Kellermann et al. 1971). At 13 cm, Broderick et al. (1971) observe ∿3.25 f.u. from (presumably) the same components. Higher resolution 13 cm data indicate a "size" ≲0".0008 (Kellermann et al. 1970), although later observations suggest either that the source has changed size or that there is structure at 13 cm (Gubbay et al. 1971). 6 cm data (Kellermann et al. 1971, corrected for some wrong d and θ values) show structure very similar to that observed here, although the coverage is not very complete. Those data support the decomposition given in Figure 4.4c by the solid lines (components B and C). The dotted lines are consistent with my results, too, but don't seem to agree with the 6 cm data; if there were components b and c at 6 cm, then there would be little variation in the visibility amplitude, contrary to observations. More observations at frequencies both higher and lower than 10.7 GHz are needed to decipher the high frequency structure of 4C 39.25.

3C 273

3C 273 was identified by Hazard et al. (1963) from a series of lunar occultations. Hazard et al. also noted the complex structure of the source at the 1" level. The redshift is 0.158 from Schmidt (1963). The source might be regarded as the original quasar, and it still keeps providing interesting data.

My visibility curves and u-v tracks are given in Figures 4.5a,b. There seem to be some systematic errors in the data, probably due to mispointing at OVRO or HRAS. For instance, the points near $IHA_{N-H} \simeq \pm 1$ are unaccountably low compared to the single value near $IHA_{N-H} = +0.2$, which is believed to be correct.

Consideration of the observed maxima and minima requires that at least three spatially separated components contribute to the observed flux density. Triple models provide a fairly good fit to the data, but there is no unique model. Two slightly resolved ($\sim$0".0005) components separated by $\sim$0".002 in PA 65° and a single unresolved source approximately halfway between (and in line) seem to be the approximate structure. The component intensity ratios are $\sim$0.60:0.20:0.20, $\pm$0.05. The central component is one of the weaker ones. The position angle of the triple model is definitely different from the position angle of the optical jet (223°). The position angle

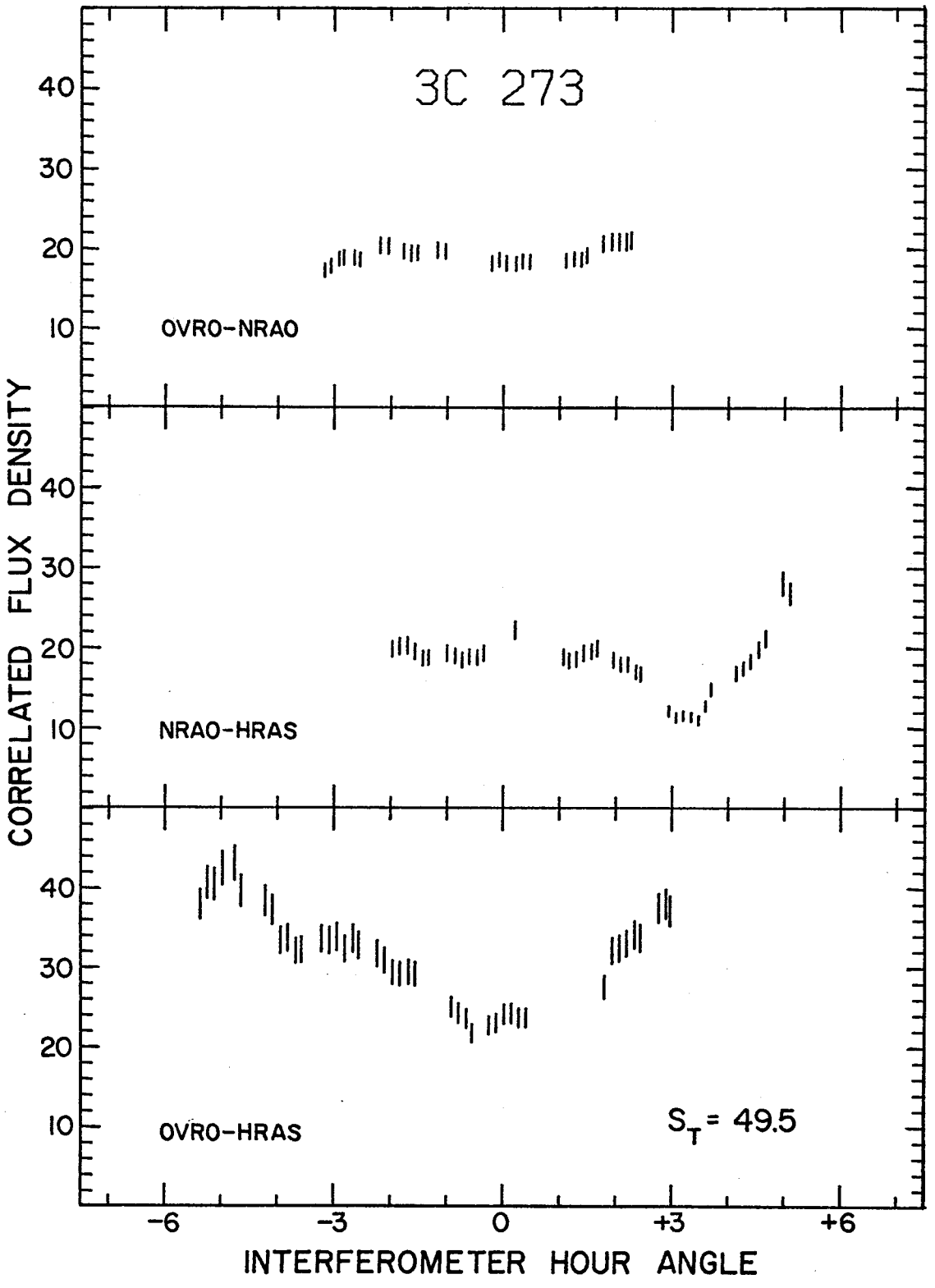

Figure 4.5a The visibility data for 3C 273. See p.28 for additional description.

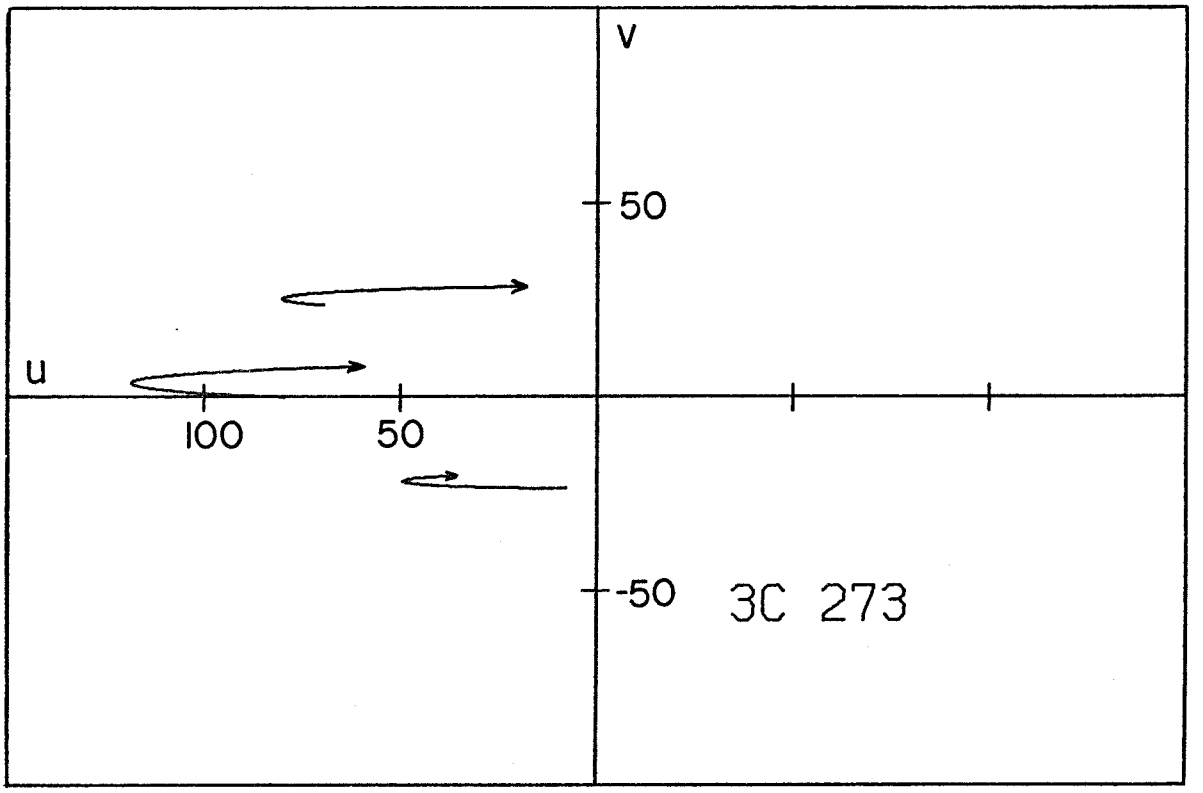

Figure 4.5b The u-v coverage for 3C 273. See p. 28 for additional description.

determined at 3.8 cm (Cohen et al. 1971) agrees with the present results.

The spectrum of 3C 273 is given in Figure 4.5c. Despite extensive high resolution observations, the compact structure of the source is not well defined, and the spectral decomposition in the figure is only schematic. The "halo" (component A) is well determined by scintillation studies (Cohen et al. 1967) and moderate resolution interferometry (Donaldson et al. 1969). The spectral index is -0.82, and the size is $\gtrsim$0".6.

VLB observations from 75 cm to 2 cm require at least 4, and probably 5, compact components for consistency with the observations. There is a $\sim$0".025 component defined by 75 cm (Clarke et al. 1969), 50 cm (Purcell 1973), and 18 cm (Kellermann et al. 1971) data. The spectrum of this component (B in Figure 4.5c) probably peaks around 1 GHz.

The 0".025 component is completely resolved at 13 cm by Broderick et al. (1972), who see an almost equal double. The double probably consists of component C and another component not drawn in for lack of corroborating information. This phantom component should produce observable effects at 18 cm. Except for one point in Figure 2a of Kellermann et al. (1971), there is no other indication of what spectral and size characteristics to assign it. I suggest a peak flux of 7-8 f.u. at $\sim$2 GHz and a size $\gtrsim$0".0025. This component may

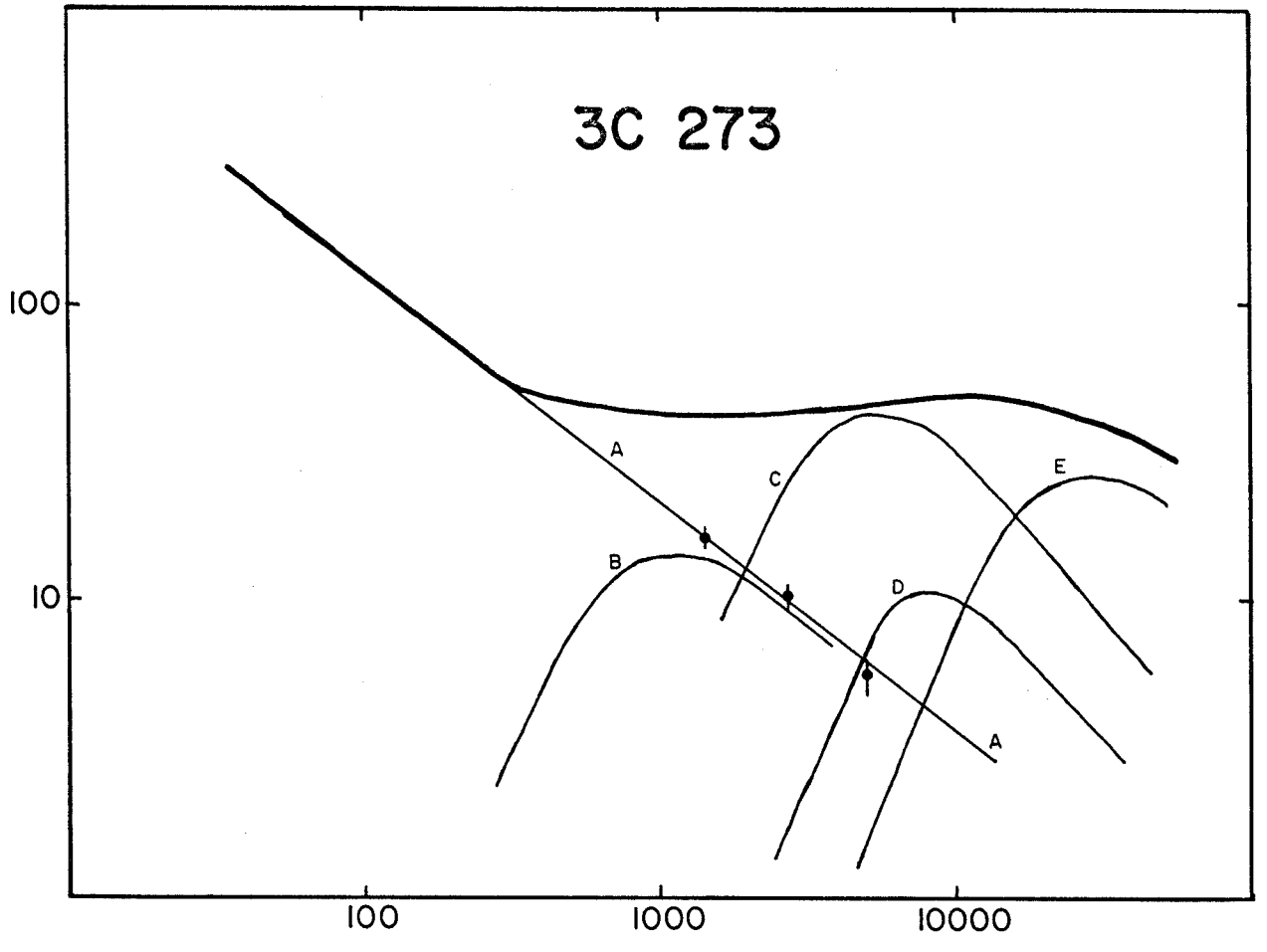

Figure 4.5c The spectrum of 3C 273, with a decomposion into several components. See p. 29 for additional description.

♦ Flux in extended component from Donaldson et al. (1969).

be interacting with components C and D to cause the low 6 cm datum at 35×10^6 λ in Figure 2b of Kellermann et al. (1971). High resolution 13 cm results (Kellermann et al. 1970) indicate a size of $\sim$0".0016 for component C, depending on how much flux is in the "phantom" component and component D at 13 cm.

Components C, D, and E have been sketched in Figure 4.5c to represent my 2.8 cm results. The spectra of these components are very uncertain. Kellermann et al. (in preparation) succesfully fit a series of 3.8 cm observations to a three component model derived from the present data. The 3.8 cm model fluxes agree fairly well for components D and E predicted from Figure 4.5c, but are too low for component C, perhaps indicating substantial resolution at 10^8 λ. Additional data at 2.8 cm and 2 cm (unpublished) should aid our understanding of 3C 273 when they become calibrated. Time variation of the structure will complicate the models, however (Whitney et al. 1971; Cohen et al. 1971).

PKS 2134+004

PKS 2134+004 was identified by Shimmins et al. (1968) as a quasar with a redshift of 1.93. They stated that the source intensity did not appear to vary with time. Longer series of observations by Dent and Kojoian (1972) and Medd et al. (1972) show only very small variations.

On all three of my baselines, the visibility amplitudes go below the detection limit, as shown in Figure 4.6a. The location of these "zeroes" are marked by circles on the u-v tracks in Figure 4.6b. The zeroes are well-determined, and a straight line connecting all three of them is impossible. Thus double or in-line multiple components are nearly ruled out (asymmetric elliptical components can give curved zero lines). It was impossible to find any simple models that fit the data. Since all the u-v tracks are essentially East-West only, component separations and position angles are highly correlated, and the fitting program could not find a good model.

The approximate structure appears to consist of two complex patches of emission of about equal strength, separated by $\sim$0".002 in a nearly East-West orientation. All the flux from the source comes from compact components. The visibility data for PKS 2134+004 are remarkably similar to those for 3C 273 (compare Figures 4.6a and 4.5a) and may

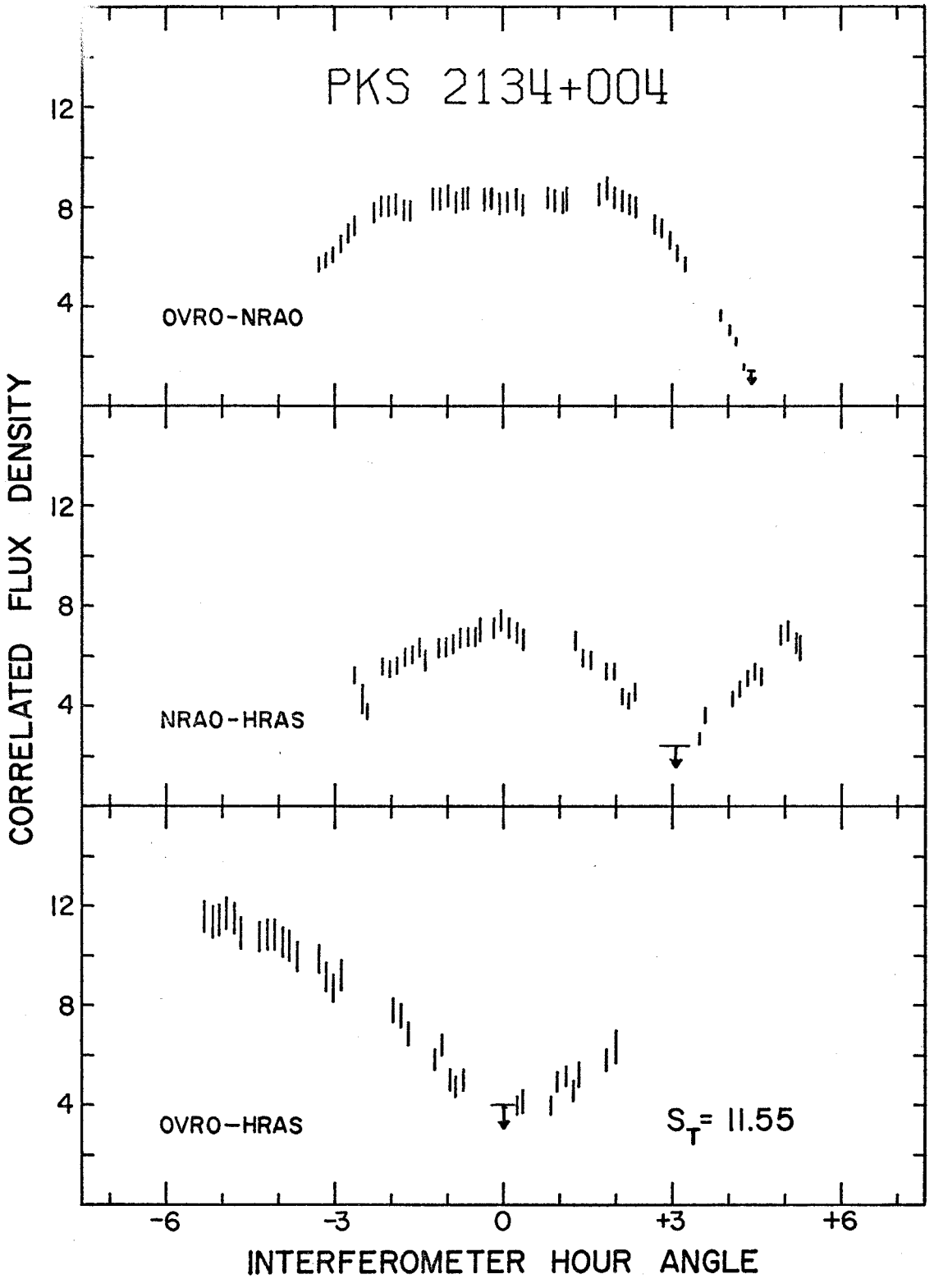

Figure 4.6a The visibility data for PKS 2134+004. See p. 28 for additional description.

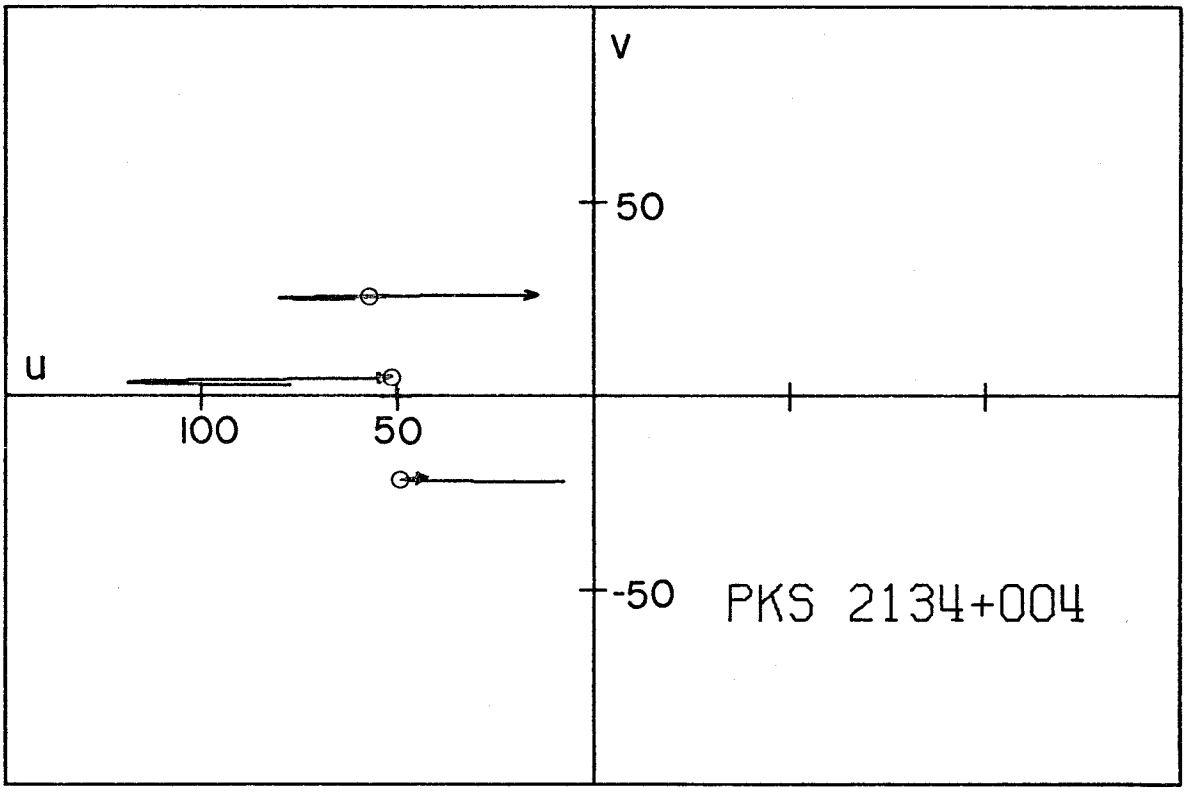

Figure 4.6b The u-v coverage for PKS 2134+004. See p. 28 for additional description.

o Visibility minima.

require a similar triple source model. If the source is basically double, the 3.8 cm data of Cohen et al.(1971) suggest a $\sim$7.5:1 intensity ratio for the components at 7.85 GHz as opposed to the near equality at 10.7 GHz. Such a rapid change of intensity ratios is possible if we are observing one component above its spectral turnover frequency and the other below its turnover. The picture may be somewhat complicated by resolution effects since Cohen et al. (1971) have observations for $\frac{d}{\lambda} > 50 \times 10^6$ only, whereas the present results have $\frac{d}{\lambda}$ as small as 20×10^6. The present results rule out the model suggested by Cohen et al. and re-emphasize the need for multiple baselines.

6 cm (Kellermann et al. 1971) and 13 cm (Kellermann et al. 1970; Broderick et al. 1972) data don't fit the simple double structure. At 13 cm, there is structure on the scale of 0".005. Another component, peaking at low frequencies (1-2 GHz), is probably required to match those observations. The 6 cm data are so scattered that it is unclear as to what the structure is at that wavelength.

Our unpublished data at 2.8 and 3.8 cm show that PKS 2134+004 has very little, if any, temporal structure variation. It seems likely that this structural stability is somehow related to the relative constancy of the total flux and spectrum (shown in Figure 4.6c). What little evidence we have indicates that flux variability and structure varia-

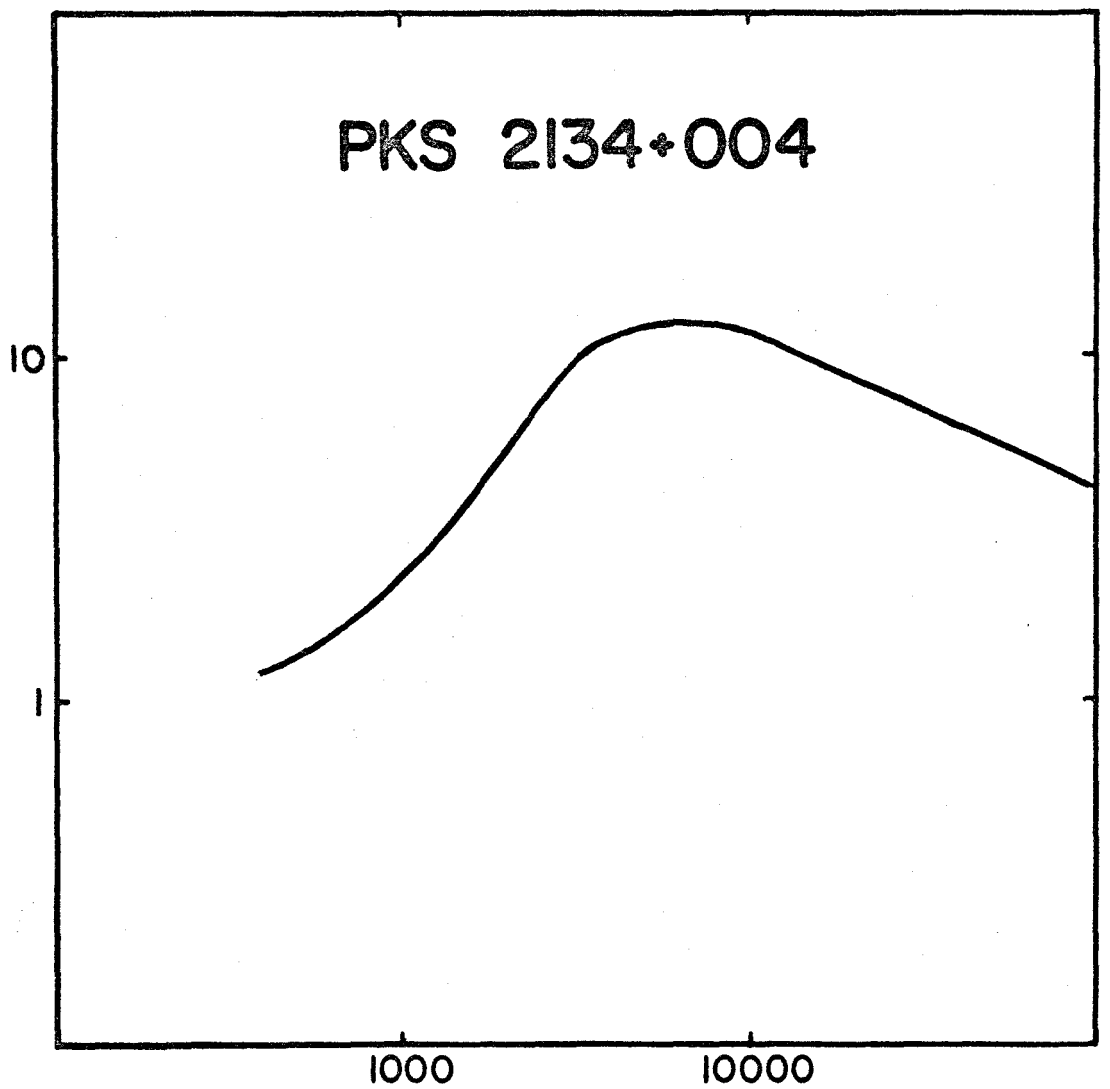

Figure 4.6c The spectrum of PKS 2134+004. See p. 29 for additional description.

bility are highly correlated, in that rapid flux variables seem to show structure variations as well. See Chapter 5 for further discussion.

OJ 287 and VRO 42.22.01

These sources are discussed together because of their similar optical and radio properties. Coincidentally, they have the least u-v coverage of any sources in this experiment, OJ 287 by design and VRO 42.22.01 by misfortune of its right ascension.

OJ 287 was identified by Blake (1970). It has extremely large and rapid optical and radio variations (Kinman and Conklin 1971; Andrew et al. 1971). High resolution observations at 3.8 cm (Cohen et al. 1971) indicated that OJ 287 was quite likely to be unresolved on all the present 2.8 cm baselines. Figures 4.7a,b,c give the visibility data, u-v tracks, and spectrum for OJ 287. Except for the unknown difficulty with the NRAO-HRAS baseline scaling (Chapter 3), the source does indeed appear structureless and unresolved. These data have been used to calibrate the correlated flux density scales as discussed in Chapter 3. The source is $\lesssim 0''.0003$ in diameter. Yen (private communication) reports that OJ 287 shows structure on a baseline of 187×10^6 λ. Our recent 2.8 cm measurements (March 1973) also indicate possible resolution at 120×10^6 λ a year after the results under discussion. It would be most interesting to look for rapid structure changes that might be correlated with total flux variations.

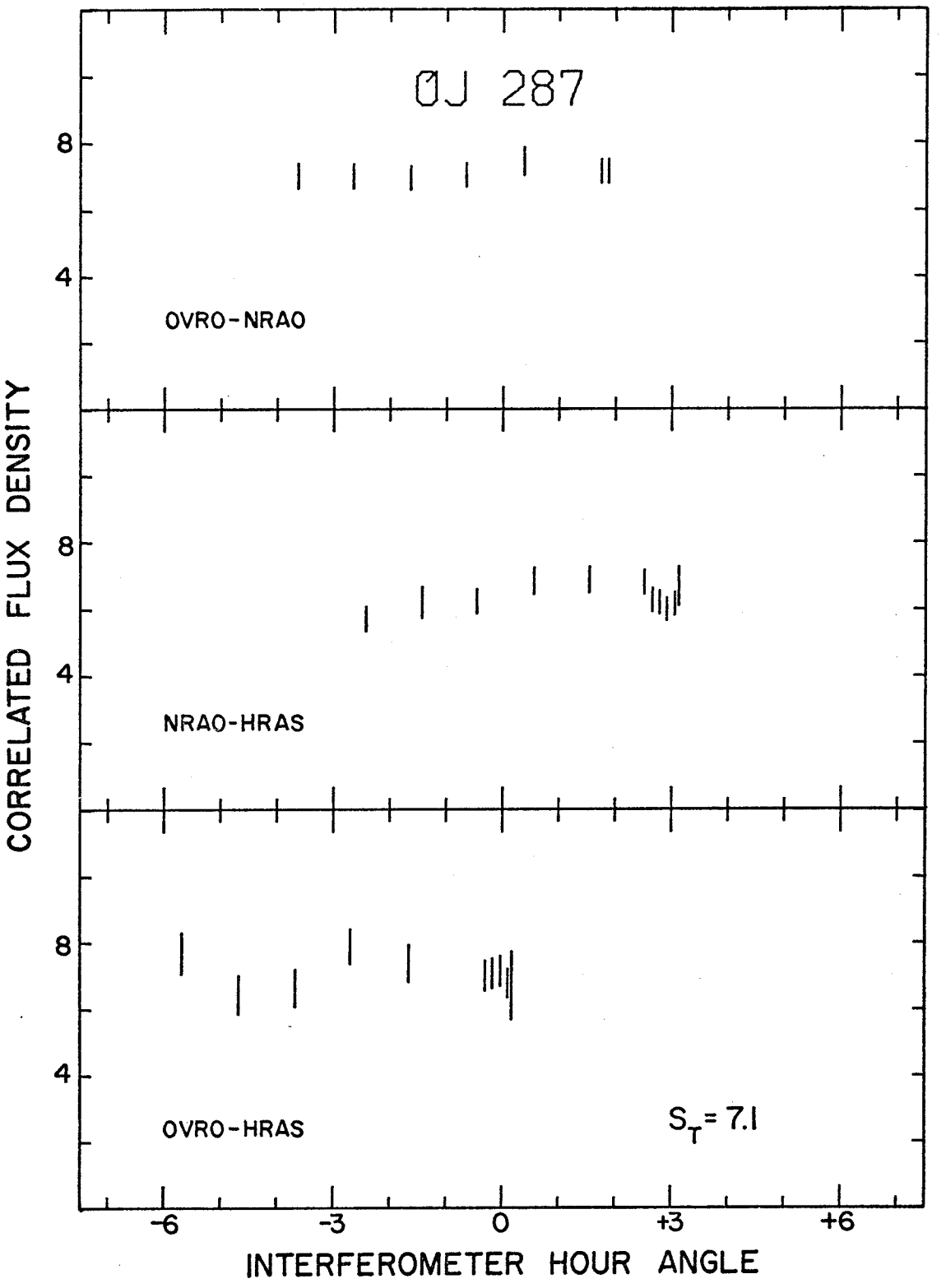

Figure 4.7a The visibility data for OJ 287. See p. 28 for additional description.

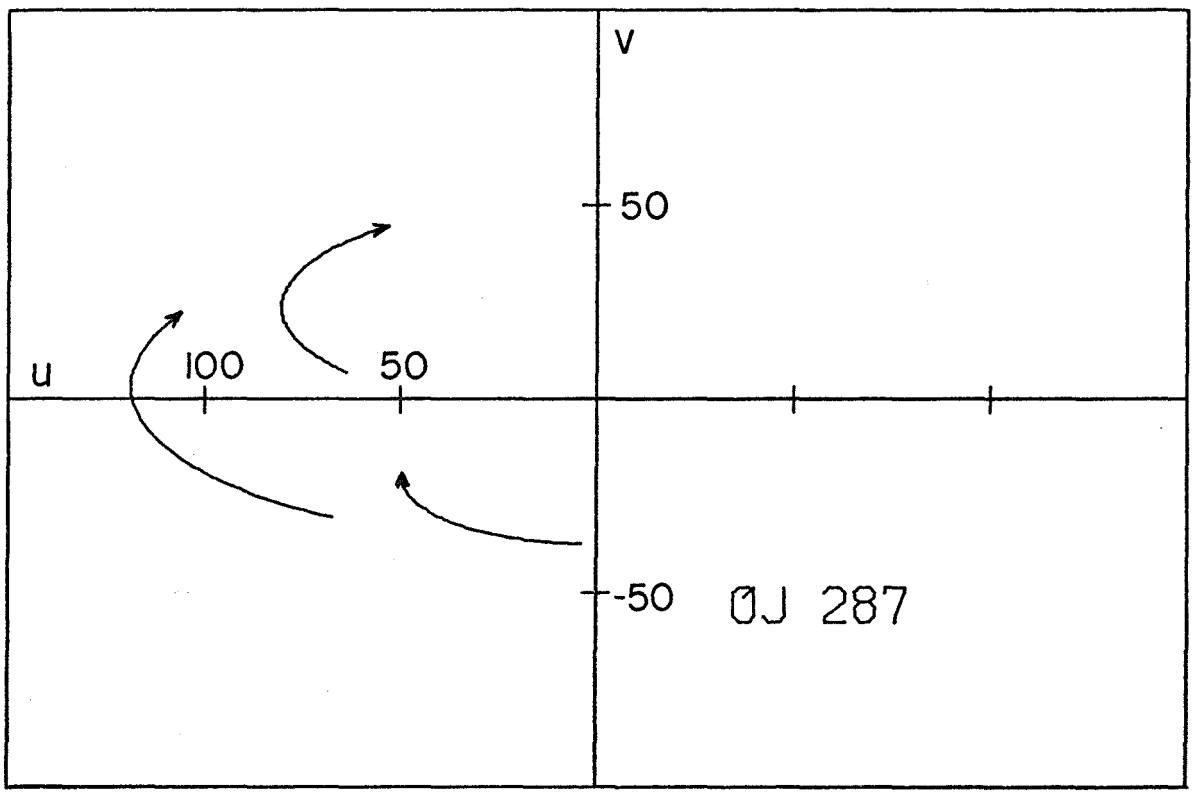

Figure 4.7b The u-v coverage for OJ 287. See p. 28 for additional description.

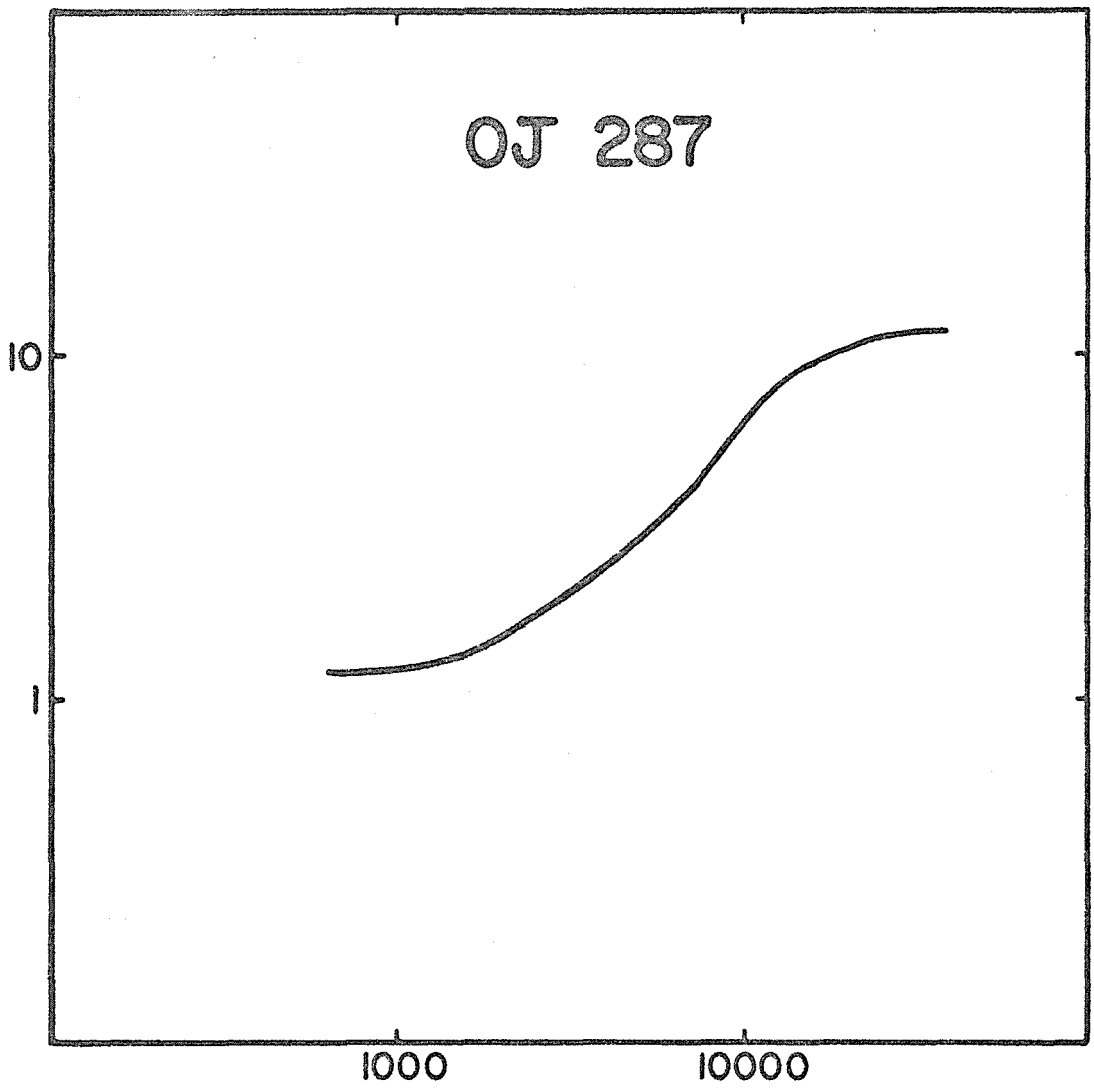

Figure 4.7c The spectrum of OJ 287. See p. 29 for additional description.

VRO 42.22.01 was identified by MacLeod and Andrew (1968) and associated with the variable "star" BL Lacertae by Schmitt (1968). Like OJ 287, VRO 42.22.01 is also a rapid optical and radio variable.

Figures 4.8a,b show the limited data and u-v coverage for VRO 42.22.01. However, there is still enough information to make a good guess at the structure. An unequal point double with 0.85 of the total flux in one component, and 0.12 in the other component, separated by 0".00135 in PA -2°, is represented by the solid line in Figure 4.8a. The separation and intensity ratios are highly correlated and uncertain by $\sim\pm0.02$ in the component intensities and $\sim\pm0".0001$ in the separation. The PA uncertainty is a few degrees. χ^2 per degree of freedom is 0.65. Higher resolution and more complete u-v coverage are necessary to better determine the parameter values, and indeed the model itself. A core-halo model was also tried, with a point core and a highly elliptical halo. The best fit, comparable to the unequal double in χ^2, occurred when the "halo" degenerated into a line. Its length was 0".0024 ± 0".0003 in PA -2°. The core contained 0.69 of the total flux, the halo 0.28.

The spectrum of VRO 42.22.01 (Figure 4.8c) gives few clues to a spectral decomposition. At 13 cm, the source is $\gtrsim$0".003 in size, with some structure (Broderick et al. 1972, 1973). An extensive series of observations at 3.8 cm shows

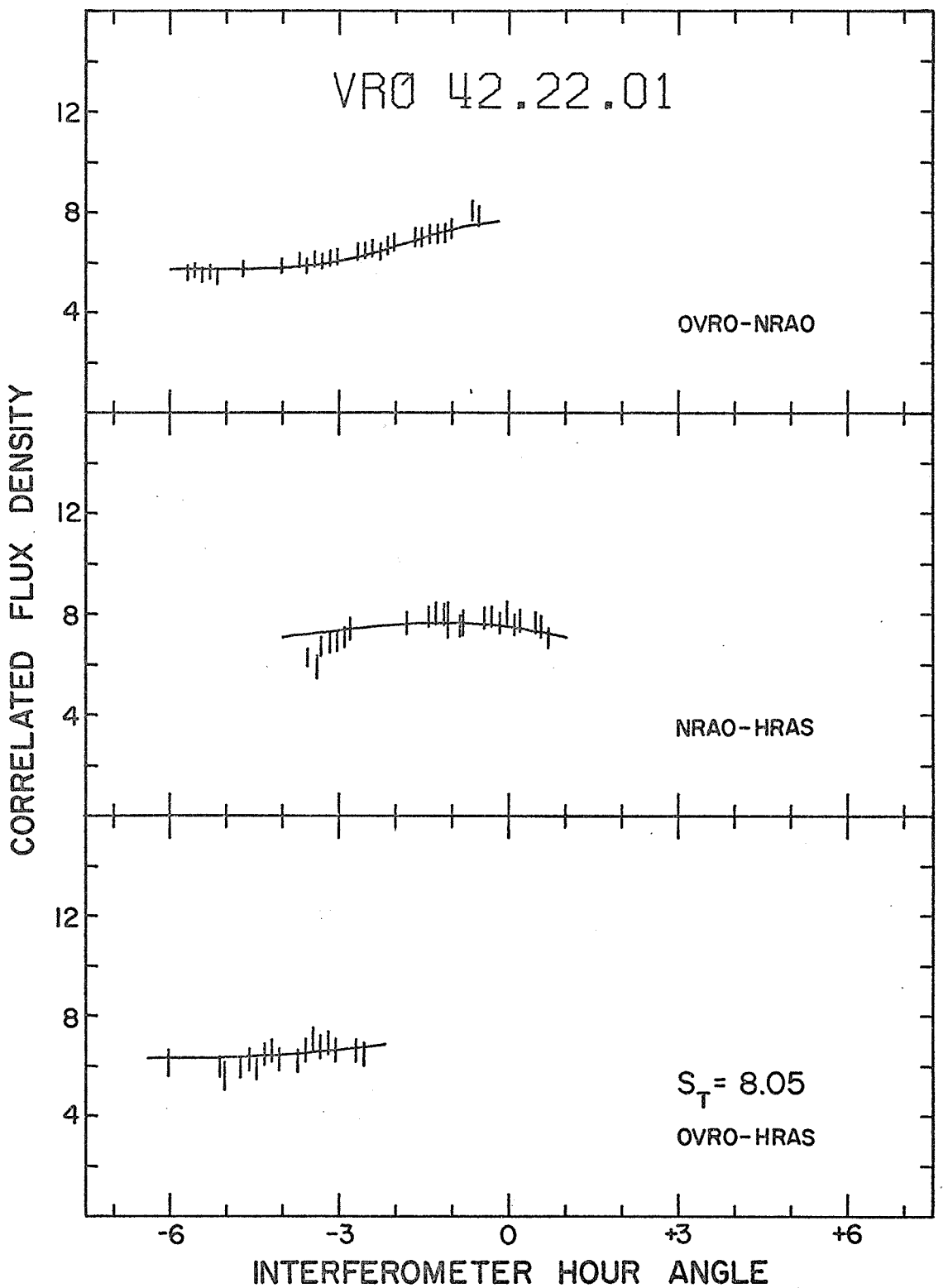

Figure 4.8a The visibility data for VRO 42.22.01. The solid line is the predicted visibility for the unequal point double discussed in the text. See p. 28 for additional description.

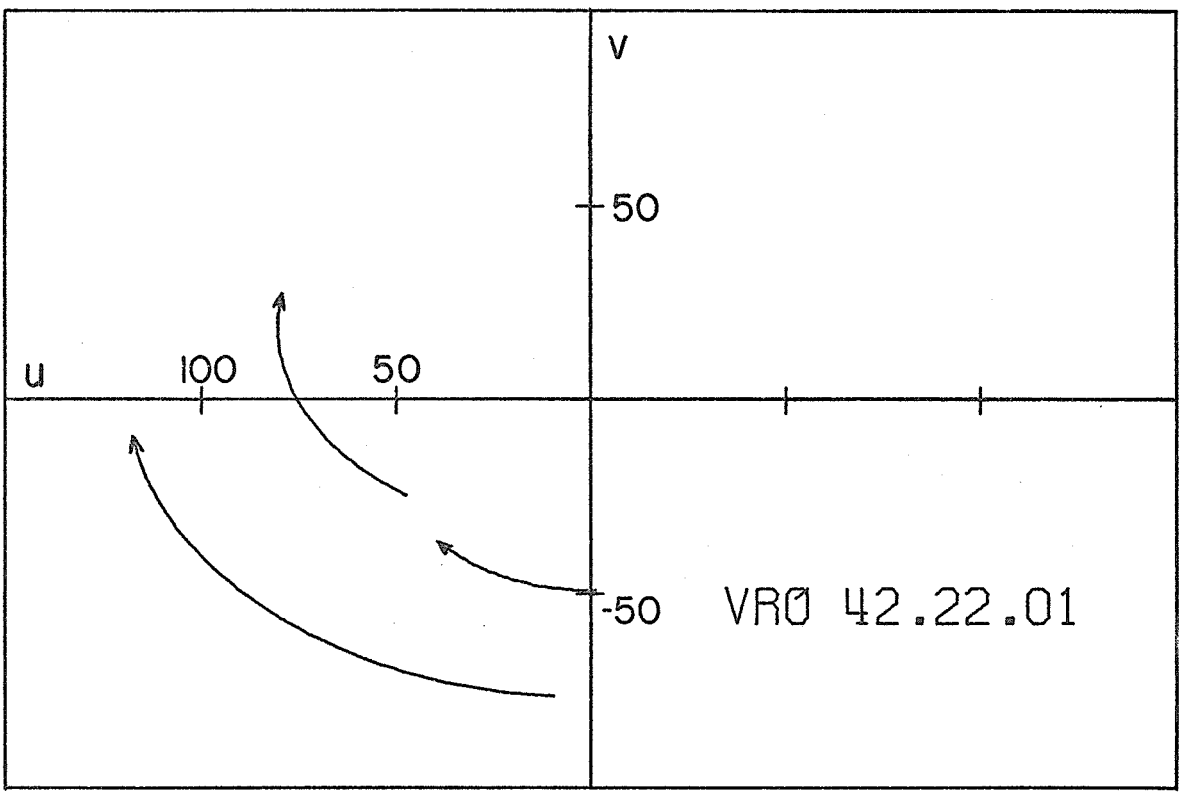

Figure 4.8b The u-v coverage for VRO 42.22.01. See p. 28 for additional description.

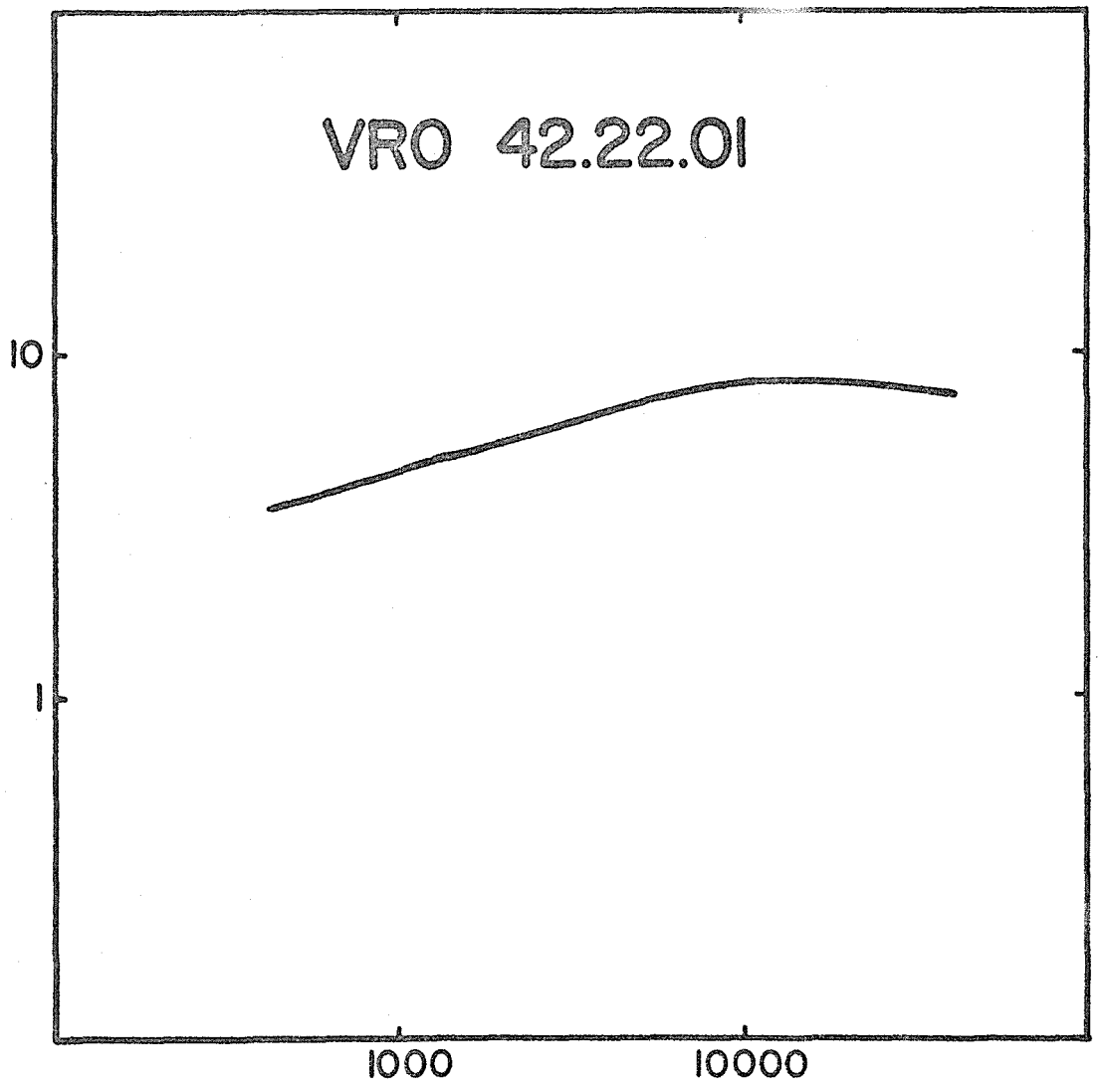

Figure 4.8c The spectrum of VRO 42.22.01. See p. 29 for additional description.

rapidly changing structure on a time scale of months (Clark et al. 1973). The position angle determined at 3.8 cm agrees very well with my results, although the maximum separation observed at 3.8 cm was somewhat smaller than the double spacing proposed here. That, however, may be an artifact of the equal double model used at 3.8 cm. Extensive monitoring at many frequencies will be necessary to understand the stuctural behavior of VRO 42.22.01.

Chapter 5. Discussion

A brief summary of the results from Chapter 4 is given in Table 5.1 along with derived physical extents and magnetic fields of the sources. The size scale given in column 4 refers to the separation of components in the double or triple models, assuming that the redshifts of the objects are reliable indicators of distance. I have used a value of 50 km sec^{-1} Mpc^{-1} for the Hubble constant and taken $q_o = +1$. The magnetic field strength in column 6 has been derived by assuming the individual components of the sources are synchrotron self-absorbed. The questions of size and magnetic field are discussed below.

A. Structure

Probably the most important result of this study is the complex structure of most, if not all, of the sources studied. As Table 5.1 indicates, multiple components are required to match the observations for 5 or 6 of the 7 sources. Our earlier observations at 3.8 cm were consistent with multiple component structure, but single elliptical components often gave equally good fits (Cohen *et al.* 1971). The present results, with slightly higher resolution and 3 baselines, rule out single elliptical component models in most cases.

Table 5.1

Modelling Results and Derived Sizes and Magnetic Fields

Source	Model	Flux in Model	Size Scale†	Component	Magnetic Field§
3C 84	≳3 Components	≳0.85*	∿8 ly	---	---
NRAO 150	Ellipse Equal double	1.00 1.00	--- ---	b B C	3×10^{-3} G $\lesssim7\times10^{-5}$ G $\lesssim2\times10^{-2}$ G
OJ 287	Point	1.00	---	---	---
4C 39.25	Unequal double	1.00	46 ly	B C b c	6×10^{-5} G 1×10^{-3} G 3×10^{-4} G 1 G
3C 273	≳3 Components	≳0.85	10 ly#	C D E	2×10^{-4} G 6×10^{-3} G $\lesssim6\times10^{-3}$ G
PKS 2134+004	≳2 Components	∿1.00*	∿40 ly	---	---
VRO 42.22.01	Unequal double Core-halo	0.97 0.95	--- ---	--- ---	--- ---

*No model, value given is flux in components ≲0".002.
†Component separation, assuming H = 50 km $sec^{-1}Mpc^{-1}$ and q_o = +1.
§Assuming synchrotron self-absorption. Upper limits are given for unresolved components by taking a diameter ≲0".0003.
#Separation between center and outer components of triple.

For 4 of the sources (3C 84, 4C 39.25, 3C 273, and PKS 2134+004), the radio radiation appears to come from spatially separate regions. I cannot rule out possible overlaps of the edges of the emission regions, but their cores seem well separated. At present, we have no way of knowing if the several components were created by a single, central event or if they arise from spatially separate outbursts in the source. Better mapping techniques and absolute position measurements might solve this problem.

For the other 3 sources, more data is necessary to determine if they have spatially separate components. VRO 42.22.01 may have a core-halo structure. In that case, the compact core is contained in a more extensive halo, and the two components may represent relatively concentric events. NRAO 150 and OJ 287 require higher resolution observations to elicit their true nature.

Although most of these sources are complex in the sense that they consist of more than one component, they in general have rather simple structure. The structure is also amazingly similar to that observed for more (by a factor of 10^4-10^5) extended sources. NRAO 150, 4C 39.25, and VRO 42.22.01 can be represented as well as the data allow ($\chi^2 \lesssim 1.0$) by models with only a few parameters. 3C 84, 3C 273, and PKS 2134+004, although not as simple, can be roughly described with just a few components. Refinements in our observing and reduction techniques will almost surely

find more complicated structure, but it will probably be only modifications to these present basic results.

Although it may be hidden by the errors in the data, there appears to be no structure seen at 2.8 cm in these sources with angular scales larger than about 0".005 (except the very extended components in 3C 84 and 3C 273). I cannot tell if some individual components have sizes ≳0".005, but if the emmision regions had such a separation and were of comparable strength, we would observe rapid "ups-and-downs" in the visibility curves. It would seem that we could detect variations that occur 4-5 times more rapidly than in 3C 84 (see Figure 4.2a). Such variations are not seen, indicating little structure on a 0".005 - 0".02 scale.

A question to ponder is the reality of the components. Do they represent physically separate entities having separate (or common) origins or are they merely concentrations in a common extended envelope. What evidence we can muster supports the concept of separate blobs of radiating material. As noted several times in Chapter 4, we have data at 18 and 13 cm that are consistent with the $\nu^{2.5}$ behavior expected for a self-absorbed synchrotron component. VLB observations of 3C 120 indicate that we are observing separate outbursts of radiation that produce expanding components with lifetimes of a year or less, and separated in space by a few light years (Kellermann et al. 1973). Time-varying radio sources provide evidence for single,

isolated outbursts. Some of these sources seem to follow the predicted behavior for a self-absorbed component very closely (Kellermann and Pauliny-Toth 1968), although others certainly do not (Medd et al. 1972).

Coordinated observations of the variation of flux and structure at many frequencies are needed to see if the several components observed at one wavelength retain their identity at another wavelength, or if there is a gradual blend of one apparent structure into a different one. The temporal variation of structure makes it difficult to compare my results with those at other frequencies. However, as noted in Chapter 4 for most of the sources, the structure seems to be the same at 2.8 and 3.8 cm. The 6, 13 and 18 cm data also seem consistent with my results in most cases.

The actual physical extent of the compact sources that I have observed is indicated in column 4 of Table 5.1. For sources with known redshift z (assuming z is a distance indicator), we can relate angular size θ and linear dimension D by

$$D = \frac{cz}{H(1+z)^2}\ \theta \qquad (5.1)$$

for a cosmology with $q_o = +1$, where H is the Hubble constant (Misner et al. 1970). Equation (5.1) predicts that D is almost proportional to θ for a wide range of redshifts:

$0.4 \lesssim z \lesssim 3.0$. Since my observations are limited to a rather narrow range of θ, it is not surprising that the sizes in Table 5.1, which are the component separations in the models, also cover only a narrow range. It may be that 10-40 l.y. is a characteristic size for the separation of components in an active quasar. All the quasars we have modelled at 2.8 and 3.8 cm have significant structure on this scale. This size, of course, corresponds to just the range of angular scale to which our experiments are sensitive and may be just a selection effect. Again, more extensive observations are necessary to decide the reality of such a "standard size".

The sizes of the individual components are harder to estimate, since most of them are only slightly resolved. In the quasars, the components are $\lesssim$10 l.y. in diameter for 4C 39.25 and PKS 2134+004 and $\lesssim$5 l.y. in diameter for the smallest components of 3C 273. In 3C 84, there is at least one component having a size less than 1 l.y. in PA 85°.

With just our small sample, complicated by selection effects, it is hazardous to attempt comparison of radio galaxy and quasar structure. Including results from 3.8 cm (Cohen et al. 1971), we can say only for our small sample that the component sizes and separations deduced for galaxies are smaller than those deduced for quasars. Since the galaxies are closer, we are most sensitive to smaller

physical sizes for the galaxies, but if they had component separations comparable to those of the quasars, we should have noticed the effect in the visibility functions. It is interesting that we find a fairly narrow range of component sizes ($\lesssim$ a factor of 10) for objects with a wide range of intrinsic luminosities, about a factor of 10^4 [$\sim(z_{max}/z_{min})^2$].

It is important to note that if the compact components are synchrotron self-absorbed, we are restricted to only a narrow range of observable parameters by the nature of our experiments. The observed flux density from a source of angular size θ is $S = \frac{2kT_b}{\lambda^2} \frac{\pi}{4} \theta^2$, where T_b is the source brightness temperature. The present results at 2.8 cm and those at 3.8 cm (Cohen et al. 1971) come from experiments at comparable wavelengths and resolutions. Thus, the measured angular sizes are also quite similar. Since most of our sources have about the same flux density, we also get results for T_b that are all about the same. The values of T_b obtained are $\sim 10^{11-12}$ °K, the maximum predicted by Kellermann and Pauliny-Toth (1969). It seems that consciously or unconsciously, we perform experiments with predictable results.

We should observe a set of weaker sources in order to determine if angular (and physical) sizes decrease with apparent flux density or remain a more-or-less constant size.

The present results argue for a relatively fixed size. State-of-the-art VLB observations could be made that would be 10 to 100 times more sensitive than those reported here. Large telescopes equipped with ultra low noise maser or cooled paramp receivers with hydrogen maser local oscillators are necessary for such measurements.

B. Classification of sources

A second important result of this study and those at 3.8 cm is that a large fraction of the high frequency radiation in these sources comes from the compact components. At least 0.85 of the total flux comes from regions less than $\sim$0".002 in diameter for the 7 sources discussed here. For those sources well-studied at 3.8 cm, $\gtrsim$0.70 of the total flux comes from compact components $\lesssim$0".001 in all cases except 3C 274 and possibly 3C 273 (Cohen et al. 1971). Thus, most of the radiation in these sources comes from a volume less than 50 light years across.

We can divide the strongest extragalactic centimeter wavelength sources (>5 f.u. at 2.8 cm) into two classes: 1) those with a "normal" spectral index ($-1.3 \lesssim \alpha \lesssim -0.5$) and extended emission regions and 2) those with flat or inverted spectra ($\alpha \gtrsim -0.5$) which are compact and time varying. 3C 274 and NGC 5128 appear to be the only exceptions. They have compact cores that contribute a few percent of the

total flux (Cohen et al. 1971, Wade et al. 1971). Going to weaker sources, the separate classes become less distinct. As well as very compact and extended sources, we will notice those sources which have less compact ($\gtrsim$0".01) components whose spectral peaks are at lower frequencies. At 10.7 GHz, those components are optically thin and have a normal spectral index. Sources which peak at 10 or 20 f.u. at frequencies less than about 1 GHz will have flux densities less than a few f.u. at 10 GHz. These sources and other weak sources which peak near 10 GHz should be observed over a wide range of resolution to look for a probable wide range of component sizes and separation.

Such measurements might provide a clue to the connection, if any, between compact sources and the classical extended radio sources. Since the luminosities of these two classes of source are quite comparable, one might naively assume that the compact sources can easily evolve into extended objects. There are at least two serious problems, however, to such an evolution. The energy reservoir for a compact source is $\sim 10^{58}$ ergs (Kellermann and Pauliny-Toth 1968), whereas a comparably luminous extended source requires $\sim 10^{60}$ ergs stored in magnetic fields and particles (Moffet 1966). Many outbursts would be required to supply sufficient energy for an extended source. Secondly, as (and if) a compact source expands, the magnetic flux is presumably conserved and the field strength would drop

as $r(t)^{-2}$. The radiating electrons also lose energy as they adiabatically "cool". Since the radiating efficiency of an electron is proportional to the product of the field and the particle energy squared, the source should fade into oblivion as it expands. Such behavior is apparently observed for some outbursts (Kellermann and Pauliny-Toth 1968). Thus it seems that compact double sources cannot grow into large double sources by themselves.

If the compact sources are the progenitors of the extended sources, there must be either some method to trap the expanding clouds of fields and electrons until they have accumulated sufficiently to start radiating again or some way to create the radiation by another process, perhaps the synchro-Compton mechanism proposed by Rees (1971). Perhaps the objects with sizes $\gtrsim$ 0".01 represent intermediate stages of condensation and radiation in the evolution to an extended object. These intermediate sized sources are too intense and stable to be the remnants of high-frequency components. It is interesting to note that the ratio of component separation to component size is nearly constant over the range $\sim$0".001 to $\sim$10'.

C. Magnetic fields

Columns 5 and 6 of Table 5.1 give the magnetic field strengths derived for several of the components resulting

from the models of Chapter 4. The component identifications in the table are the same as those in the appropriate spectrum illustrations in Chapter 4. The fields B, in Gauss, have been calculated from $B = 2.5 \times 10^{-8} \frac{\nu^5 \theta^4}{S^2(1+z)}$, where ν is the frequency (in MHz) of the peak flux density S (in f.u.) of a given component of size θ (in arcsec) in a source with redshift z (Terrell 1966). A value of $z = 1$ was assumed for NRAO 150. The values of B in the table have rather large errors because of the high powers of ν and θ. The errors are probably about an order of magnitude.

Except for component c of 4C 39.25, the values of the fields are $\sim 10^{-3\pm1}$ gauss. This is slightly higher than the results of Kellermann and Pauliny-Toth (1969), and may be attributed to the higher frequencies found here for ν. In general, the derived fields are less than the equipartition value (for which the total magnetic field energy equals the total particle energy), as is derived below for 4C 39.25. Thus, it seems likely that the pressure of the radiating particles will cause the compact components to expand, unless they are confined by some external medium. Future observations should confirm or deny expansion of the individual components. Higher resolution than used here is desirable, since many of the components are barely resolved. We

probably have observed the expansion of components in 3C 120 (Kellermann et al. 1973).

The assumption that we are observing synchrotron self-absorbed (SSA) components is fundamental to the above discussion. We should investigate other possible mechanisms for producing "low" frequency spectral turnovers before placing too much confidence in the SSA assumption. Free-free absorption by an intervening thermal plasma or the suppression of low frequency radiation by a plasma containing the relativistic synchrotron electrons could produce a spectral turnover.

Free-free absorption can probably be ruled out by the extremely sharp low frequency cut-off it would produce. Since any postulated cloud of plasma must be fairly compact itself (we would see its radiation otherwise) and the brightness temperature of a compact source ($\sim 10^{11-12}$°K) is much greater than the $\sim 10^{4}$°K expected for a thermal plasma, we need only consider the effect of absorption of the emission from the compact source. The absorption coefficient of a thermal plasma is proportional to ν^{-2}. Thus, we would expect the flux density of the absorbed source to go as $e^{-\nu^{-2}}$ below the cut-off frequency. As noted in Chapter 4, the data for NRAO 150 and 4C 39.25 are consistent with a $S_\nu \propto \nu^{2.5}$ behavior. An exponential cut-off is not compatible with the observations.

Suppression of low frequency radiation by a plasma (optically thin) which contains the radiating electrons also produces an extremely steep spectrum below the turn-over frequency (Pacholczyk 1970). Again, the data are incompatible with such a spectrum. An even stronger case against such a mechanism can be made by calculating the expected Faraday rotation the plasma would cause. The suppression would become important for frequencies $\lesssim 20 \frac{n_e}{B}$, where n_e is the thermal electron density per cm^3 (Ginzburg and Syrovatskii 1965). For a turn-over frequency of 10 GHz, $n_e \simeq 5 \times 10^3$ to 5×10^7 is necessary to cause any such effect for magnetic fields of 10^{-5} G (the "classical" value for extended sources) to 10^{-1} G (the approximate equipartition value for the compact sources).

The internal Faraday rotation measure of the linear polarization from a source of radius r (in pc) is $\sim 8.1 \times 10^5 n_e B r$. For the values of n_e and B given above and a value of $r \simeq 1$, we predict rotation measures of 4×10^4 to 4×10^{12}. These rotation measures are grossly in excess of the maximum observed for any source and rule strongly against the existence of moderately dense plasma within the source. Thus synchrotron self-absorption remains as the likely cause of spectral turnover.

D. 4C 39.25

Of the 7 sources studied here, only 4C 39.25 has both

a well-determined model and a redshift. With the proposed spectral decomposition, we can find the luminosity and equipartition magnetic field for the components. The calculations below refer to components B and C of Figure 4.4c.

The total flux of the components may be found by integrating the spectrum to some high-frequency limit. I have used 100 GHz as this limit because there are no higher frequency measurements. Hence, the derived luminosities will be lower limits, as will the values of the equipartition magnetic fields. The total flux of component B is $\sim 6 \times 10^{-16}$ Wm^{-2}. Component C has flux $\sim 6 \times 10^{-15}$ Wm^{-2}. For a Hubble constant of 50 km sec^{-1} Mpc^{-1} and $q_o = +1$, the resultant luminosities are $\sim 10^{38}$ watts for component B and $\sim 10^{39}$ watts for component C.

If we make the simplifying assumptions that monoenergetic electrons produce the observed radiation and that the peak of their radiation spectrum coincides with the peak of the observed spectra, we can estimate the equipartition magnetic fields. By relating the magnetic field energy, the volume and luminosity of the source, the frequency of the spectral peak, and the radiation efficiency of the electrons, we find $B_e^{3.5} \simeq 1.4 \times 10^{20} \frac{L}{V\nu^{0.5}}$ for the equipartition field, where L is the source luminos-

ity in watts, V is the source volume in cm^3, and ν is the peak frequency of the spectrum in Hz. For 4C 39.25, $B_e \simeq$ 0.1 gauss for both components, assuming that they are spherically symmetrical and their radii are $\sim$5 l.y.

This value for B_e is significantly greater than the values in Table 5.1. Thus it appears that the particle energy dominates, and the pressure of the particles should cause individual components to expand unless there is an external restraining force. In 4C 39.25, the components have radii of $\sim$5 l.y., so they must be at least 5 years old, and possibly much older. Whether or not we observe the components to expand depends on their expansion velocity and our time base for comparison. If the components are expanding relativistically in their own frame, the apparent size can change more rapidly than the speed of light (Rees 1967), and we might expect to observe significant changes in a year or two (or less). If the components are expanding slowly, the fractional expansion per year will be small ($\sim\frac{1}{5}\frac{v}{c}$ for a radial velocity of expansion v) and observations many years apart will be necessary to discern any meaningful changes.

Additional unpublished observations of 4C 39.25, taken 5 and 10 months after the present results, show little, if any, change in the size or separation of the components. Similarly stable structure obtains for NRAO 150 and

PKS 2134+004. These three sources also show only small, slow changes in their total flux density (Medd et al. 1972). Conversely, 3C 120, 3C 273, 3C 279, and VRO 42.22.01 show rapid variations in flux and structure (Cohen et al. 1971; Whitney et al. 1971; Clark et al. 1972; Shaffer et al. 1972; Kellermann et al. 1973; Shapiro et al. 1973). Conditions in the rapidly varying sources may promote the frequent creation of short-lived (rapidly expanding) components. These outbursts, if spatially separate, would make the source structure variable on a short time scale. The stable sources probably evolve slowly, in the relative absence of outbursts. Observations with a long time base are needed to look for these slow variations.

E. Suggestions for further work

The results presented here represent the first of a series of observations. We have already carried out 4 additional experiments using these three antennas, as well as others. As noted above, some sources seem to have stable structure while others show rapid variation. Continued observations should improve our knowledge of source structure and its variation. Efforts should be made to find any correlations between structure variability and flux variations. With only a small sample, there appears to be a good correlation between the existence of such varia-

tions, but the nature of the relationship is not at all established.

Improved modelling techniques are needed to better understand our sources. Our limited imagination in the Fourier transform plane restricts the classes of models used and may be giving us misleading results. Bates and Napier (1972) describe a technique for "inverting" data with very noisy phases. Perhaps their method can be extended to work without any phase information at all. However, Rogstad (1968) has shown that phase information can be recovered from an array of antennas. His method seems applicable to VLB observations. It would than be possible to do a standard inversion. Such results, uncontaminated by the model-fitter's prejudices, would greatly refine our knowledge of compact structure.

All of the models presented in Chapter 4 require confirmation by observations at nearby frequencies and higher resolution. The spectral decompositions in Chapter 4 lead to firm predictions for the results of new observations.

4C 39.25 should be observed at 5 GHz and lower frequencies. At 5 GHz, components A and B (see Figure 4.4c) should make an almost equal double, whereas components b and c would appear as a very unequal double dominated by component b. Low frequency (400-1000 MHz) data are needed to prove or disprove the postulated low frequency compact

component.

The multitude of components that apparently exist in 3C 273, as shown in Figure 4.5c, make predictions difficult. Perhaps we should accummulate more observations at many frequencies and resolutions before committing ourselves. 18, 13, and 6 cm results with good (u,v)-plane coverage are vitally needed.

Higher resolution observations should allow a choice between the two models for NRAO 150. As the visibility function is measured to lower values of γ, the differences between models become more obvious. If the source is double, we should see a definite minimum. Observations at nearby frequencies should better define the spectra of the two possible components. Similarly, we should try to find a minimum in the VRO 42.22.01 visibility function. If it exists, it would be strong support for the double model. Observations at other frequencies should allow a spectral decomposition, although the rapid variations of flux density will make things difficult. Perhaps we will find a variable component and a lower frequency, rather stable, component.

Very accurate observations at lower frequencies are very important in providing (or denying) support for the synchrotron self-absorption theory of compact components. Data at 21, 18, and 13 cm should be capable of defining the

optically thick part of the component spectra. Current data are consistent with the expected $\nu^{2.5}$ behavior but don't rule out some other relation.

Better calibration is desirable at 2.8 cm as well. The present calibration accuracy seems to be about 5%, neglecting the question of absolute scale. The forthcoming installation of a cooled paramp at OVRO should permit accurate calibration of antenna gain and system temperature comparable to that achieved at NRAO. The problem of pointing and gain calibration at HRAS will remain, however. The Fort Davis dish is being pushed very hard for operation at 2.8 cm. A cooled receiver and/or new antenna would be highly desirable but probably beyond the realm of possibility. The data acquisition systems would be greatly improved by the addition of new tape recorders. Prolonged exposure to the idiosyncrasies of the VR-660C's is probably hazardous to one's mental health. It is currently impossible to process the same data twice and get the exact same answer. The stability of the bit streams recovered from the recorded data seems subject to various vagaries, which fortunately average out (usually!). Unfortunately, the inertia of the $200,000-$300,000 currently invested in the Mk II system may be hard to overcome.

Lower resolution work at 2.8 cm is also desirable (despite the continual plea above for higher resolution).

First of all, we should search for more extended sources that peak near 2.8 cm, or for the faint debris that may be left after a high frequency outburst has evolved considerably. We may find some missing link between the two classes of compact and extended sources proposed earlier. Additionally, on angular scales of 0".002 to 0".05, we should be able to observe the optically thin part of the spectra of the many sources that have relatively large components. It may be possible to see effects of evolution on these presumably older objects.

Appendix

Noise statistics and low signal-to-noise ratio

Noise statistics: For a small cross-correlation coefficient ρ, Purcell (1973) has shown that the rms error in one N-bit estimate of ρ is $\sigma_\rho = 1/\sqrt{N}$. For a 15-second integration and a 4 MHz bit rate, $N = 60 \times 10^6$ and $\sigma_\rho = 0.00013$. The validity of this derivation may be checked empirically by plotting a histogram of 15-second VLBAMP (Clark et al. 1972) cross-correlation amplitudes. The results are shown in Figure A.1 for one hour of data that appeared to represent a constant correlation amplitude. The histogram has a Gaussian shape, as expected, with a dispersion $\sigma = 12.4$[1], in very good agreement with the 13 predicted above. Similar profiles were obtained for several other sets of data, over a wide range of mean values. There is a slight trend for σ_ρ to increase with correlation amplitude (for example, $\sigma_\rho \simeq 16$ for $\rho \simeq 330$). This is probably an effect of the amplitude fitting procedure (Clark et al. 1972).

---

[1]It is more convenient to use correlation units, which are 10^5 times the actual correlation values.

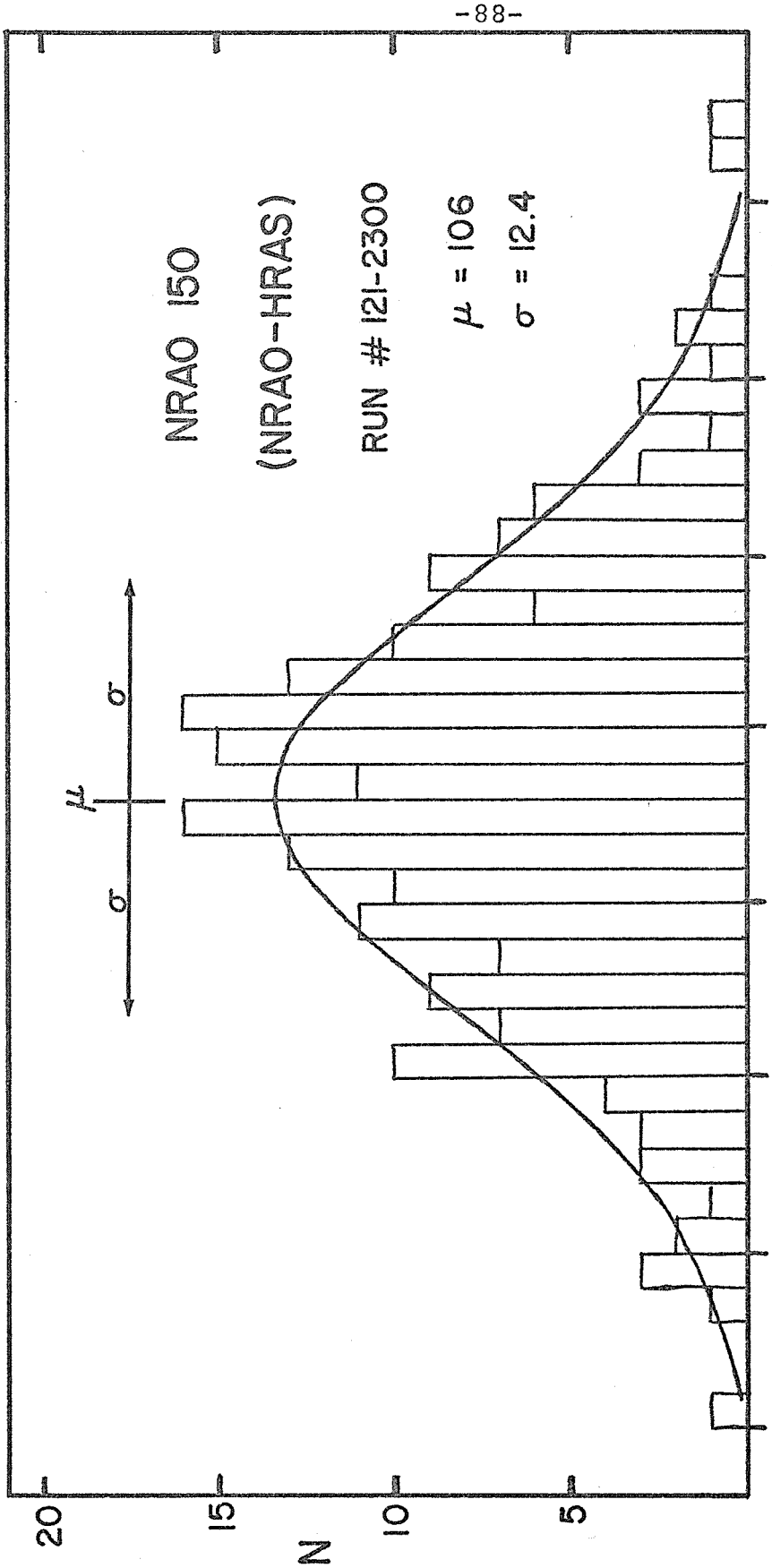

Figure A.1 Distribution of 15-second integrations from VLBAMP. The solid line is a Gaussian with the same area, mean, and dispersion as the histogram.

With the appropriate scaling factors for the various baselines, $\sigma_\rho = 13$ implies an rms error (ΔS) in the correlated flux density of $\sim$0.43, $\sim$1.0, and $\sim$1.7 f.u. for a 15-second integration for the OVRO-NRAO, NRAO-HRAS, and OVRO-HRAS baselines respectively. These are typical values and vary somewhat with the corrections for antenna gain and system temperature.

For an incoherent average of t seconds of 15-second coherent integration data, an error in the correlated flux density of $\sigma_s = \frac{\Delta S}{\sqrt{t/15}}$ has been assigned. This value of σ_s and the 5% calibration error (5% of the correlated flux density--see Chapter 3) have been added in quadrature to give the final error estimates for all the data, as plotted in the visibility curves in Chapter 4.

Low signal-to-noise ratio effects: As discussed by Purcell (1973), the computer program (VLBAMP) that determines the correlation coefficient for each coherent integration period systematically overestimates the amplitudes. For large signal-to-noise ratios (SNR's), the overestimate is the difference between a Rayleigh and a Gaussian distribution. For a SNR greater than 5[1], the difference between the two distributions is less than 2% and decreases with increasing

---

[1]The SNR = μ/σ for a Gaussian distribution $P(x,\mu,\sigma) = (2\pi\sigma^2)^{-1}\exp[-(x-\mu)^2/2\sigma^2]$ (Bevington 1969).

SNR. Compared to noise and calibration errors, an effect of this size is small and has been ignored.

For small SNR's, another problem arises. VLBAMP searches for the largest value of (presumed) signal+noise from a grid of Fourier coefficients calculated for several time delays and fringe rates in the vicinity of the expected signal. Many of these coefficients represent only noise, but they may be larger than the values of signal+noise for a weak signal. Thus, in its quest, VLBAMP may pick a coefficient that represents only noise when searching for a weak signal. The net effect is an overestimation of the correlation coefficient when several integrations are averaged. Although interpolation smears the distinction (Clark et al. 1972), it is a good approximation to assume that VLBAMP picks values from either a distribution of signal plus noise or a distribution of noise only. If we can identify these two distributions, we can determine their effect on the average result and correct for it.

The signal-plus-noise distribution was taken to be a Gaussian. For a SNR = 3 (the lower limit for meaningful results) the difference in the mean between Rayleigh and Gaussian distributions is $\sim$8%, but this is less than or comparable to the statistical noise and has again been ignored. The noise-only distribution was determined empirically from data with little or no signal present. Figure A.2 shows the

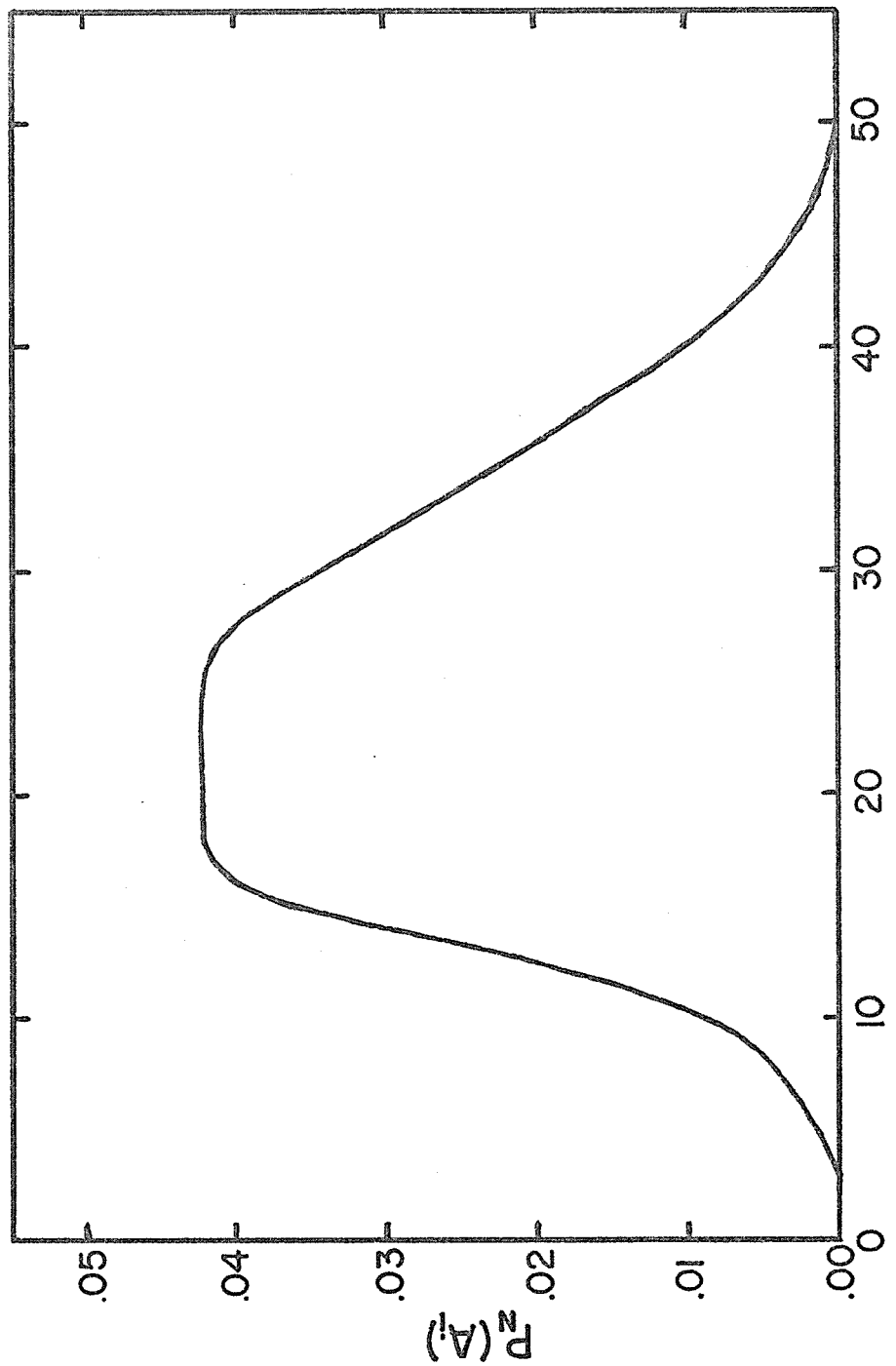

Figure A.2 Probability distribution of noise values from VLBAMP. (15-second integrations, forced LSB)

smoothed, normalized noise-only probability distribution that resulted.

In the following discussion, A_i represents the ith value of the correlation coefficient determined by VLBAMP in a series of coherent integrations which are averaged to give a mean value μ. My correction scheme consists of the following steps: 1) for all possible values of A that the A_i may take, determine the number of times such a value was chosen from the noise-only distribution, 2) determine what value should have been chosen from the signal-plus-noise distribution, and 3) correct the mean value for the average overestimate.

For n values of the correlation coefficient, we get an estimate of the mean value $\mu = \frac{\sum A_i}{n}$. Then, assuming a Gaussian distribution for the A_i (not strictly correct), the probability of finding an amplitude less than a given A is

$$P(A<A) = \frac{1}{\sqrt{2\pi\sigma^2}} \int_{-\infty}^{A} e^{-(A-\mu)^2/2\sigma^2} \, dA \quad . \qquad (A.1)$$

(Letting the lower limit of the integral go to $-\infty$, rather than 0, makes a negligible error.) Calling $P_N(A)$ the probability of chosing a value of A from the noise-only distribution, we find the joint probability that the signal-plus-noise value is less than A and that VLBAMP picked a noise-only value of A to be $P(A<A) \cdot P_N(A)$. For n integrations, there will be $nP(A<A)P_N(A)$ noise-only values in the estimate of the mean.

Given that a sample from the noise-only distribution was chosen, we can find the expected value that should have been taken from the signal-plus-noise distribution. The expectation value of A, given that A<*A*, is

$$E(A|A<A) = \frac{\int_{-\infty}^{A} Ae^{-(A-\mu)^2/2\sigma^2}\, dA}{\int_{-\infty}^{A} e^{-(A-\mu)^2/2\sigma^2}\, dA} \quad . \qquad (A.2)$$

Thus, in the summation for μ, we have added *A* rather than $E(A|A<A)$ for the $nP(A<A)P_N(A)$ times that VLBAMP selected an amplitude from the wrong distribution. Taking the difference, over all possible values of *A*, we find a corrected mean of $\mu' = \mu + \sum_A P(A<A)\cdot P_N(A)\cdot[E(A|A<A) - A]$. A slightly better estimate might result if this process were repeated, using μ' in equations (A.1) and (A.2) in place of μ.

The correction is easily calculated using computer error function subroutines (hence the desire to avoid Rayleigh distributions) for the integrals. For σ = 12, Table A.1 gives representative values for the corrected mean correlation coefficient, for 15-second integrations.

Table A.1

Correction for Noise Bias
(15-second integrations)

Mean VLBAMP Correlation Coefficient (μ)	Corrected Mean Correlation Coefficient (μ')
>58	No change
55	54.9
50	49.8
45	44.5
40	38.9
35	33.0

REFERENCES

Adgie, R. L., Crowther, J. H., and Gent, H. 1972, *M.N.R.A.S.*, 159, 233.

Andrew, B. H., Harvey, G. A., and Medd, W. J., 1971, *Ap. Letters*, 9, 151.

Artyukh, V. S., Vitkevich, V. V., Dagkesemanskii, R. D., and Kozhukhov, V. N. 1969, *Soviet Astr.—AJ*, 12, 567.

Bare, C., Clark, B. G., Kellermann, K. I., Cohen, M. H., and Jauncey, D. L. 1967, *Science*, 157, 189.

Bates, R. H. T. and Napier, P. J. 1972, *M.N.R.A.S.*, 158, 405.

Berge, G. L. and Seielstad, G. A. 1972, *A.J.*, 77, 810.

Bevington, P. R. 1969, *Data Reduction and Error Analysis for the Physical Sciences*, (New York: McGraw-Hill).

Blake, G. M. 1970, *Ap. Letters*, 6, 201.

Broderick, J. J., Kellermann, K. I., Shaffer, D. B., and Jauncey, D. L. 1972, *Ap. J.*, 172, 299.

Broderick, J. J., Jauncey, D. L., Kellermann, K. I., and Yerbury, M. 1973 (private communication).

Broten, N. W., Legg, T. H., Locke, J. L., McLeish, C. W., Richards, R. S., Chisholm, R. M., Gush, H. P., Yen, J. L., and Galt, J. A. 1967, *Science*, 156, 1592.

Broten, N. W., Clarke, R. W., Legg, T. H., Locke, J. L., Galt, J. A., Yen, J. L., and Chisholm, R. M. 1969, *M.N.R.A.S.*, 146, 313.

Clark, B. G. 1973, *Proc. I.E.E.E.*, in press.

Clark, B. G., Weimer, R., and Weinreb, S. 1972, *NRAO Electronics Division Internal Report 118.*

Clark, B. G., Kellermann, K. I., Cohen, M. H., Shaffer, D. B., Broderick, J. J., Jauncey, D. L., Matveyenko, L. I., and Moiseev, I. G. 1973, *Ap. J. (Letters)*, 182, L57.

Clarke, R. W., Broten, N. W., Legg, T. H., Locke, J. L., and Yen, J. L. 1969, *M.N.R.A.S.*, 146, 381.

Cohen, M. H. 1972, *Ap. Letters*, 12, 81.

Cohen, M. H. 1973, *Proc. I.E.E.E.*, in press.

Cohen, M. H., Gundermann, E. J., and Harris, D. J. 1967, *Ap. J.*, 150, 767.

Cohen, M. H., Cannon, W., Purcell, G. H., Shaffer, D. B., Broderick, J. J., Kellermann, K. I., and Jauncey, D. L. 1971, *Ap. J.*, 170, 207.

Dent, W. A. 1965, *Science*, 148, 1458.

Dent, W. A. and Kojoian, G. 1972, *A. J.*, 77, 819.

Dent, W. A. and Hobbs, R. W. 1973, *A. J.*, 78, 163.

Donaldson, W., Miley, G. K., Palmer, H. P., and Smith, H. 1969, *M.N.R.A.S.*, 146, 213.

Elgaroy, O., Morris, D., and Rowson, B. 1962, *M.N.R.A.S.*, 124, 395.

Erickson, W. C. and Cronyn, W. M. 1965, *Ap. J.*, 142, 1156.

Ginzburg, V. L. and Syrovatskii, S. I. 1965, *Ann. Rev. Astr. and Ap.*, 3, 297.

Gubbay, J. S., Legg, A. J., Robertson, D. S., Moffet, A. T., and Shaffer, D. B. 1971 (private communication).

Hazard, C., Mackey, M. B., and Shimmins, A. J. 1963, *Nature*, 197, 1037.

Humason, M. L., Mayall, N. U., and Sandage, A. R. 1956, *A. J.*, 61, 97.

Kellermann, K. I. and Pauliny-Toth, I. I. K. 1968, *Ann. Rev. Astr. and Ap.*, 6, 417.

Kellermann, K. I. and Pauliny-Toth, I. I. K. 1969, *Ap. J. (Letters)*, 155, L71.

Kellermann, K. I., Pauliny-Toth, I. I. K., and Williams, P. J. S. 1969, *Ap. J.*, 157, 1.

Kellermann, K. I., Clark, B. G., Jauncey, D. L., Cohen, M. H., Shaffer, D. B., Moffet, A. T., and Gulkis, S. 1970, *Ap. J.*, 161, 803.

Kellermann, K. I. and Pauliny-Toth, I. I. K. 1971, *Ap. Letters*, 8, 153.

Kellermann, K. I., Jauncey, D. L., Cohen, M. H., Shaffer, D. B., Clark, B. G., Broderick, J., Rönnäng, B., Rydbeck, O. E. H., Matveyenko, L., Moiseyev, I., Vitkevitch, V. V., Cooper, B. F. C., and Batchelor, R. 1971, *Ap. J.*, 169, 1.

Kellermann, K. I., Clark, B. G., Jauncey, D. L., Broderick, J. J., Shaffer, D. B., Cohen, M. H., and Niell, A. E. 1973, *Ap. J. (Letters)*, 183, L51.

Kellermann, K. I., Clark, B. G., Shaffer, D. B., Cohen, M. H., Jauncey, D. L., Broderick, J. J., and Niell, A. E. 1974 (in preparation).

Kinman, T. D. and Conklin, E. K. 1971, *Ap. Letters*, 9, 147.

Knight, C. A., Robertson, D. S., Rogers, A. E. E., Shapiro, I. I., Whitney, A. R., Clark, T. A., Goldstein, R. M., Marandino, G. E., and Vandenberg, N. R. 1971, *Science*, 173, 52.

Kraus, J. D. and Andrew, B. H. 1970, *Ap. J. (Letters)*, 159, L41.

Legg, T. H., Broten, N. W., Fort, D. N., Yen, J. L., Bale, F. V., Barber, P. C., and Quigley, M. J. S. 1973, *Nature*, 244, 18.

Lynds, R. 1970, *Ap. J. (Letters)*, 159, L151.

Lynds, C. R., Hill, S. J., Heere, K., and Stockton, A. N. 1966, *Ap. J.*, 144, 1244.

MacDonald, G. H., Kenderdine, S., and Neville, A. C. 1968, *M.N.R.A.S.*, 138, 259.

MacLeod, J. M. and Andrew, B. H. 1968, *Ap. Letters*, 1, 243.

Medd, W. J., Andrew, B. H., Harvey, G. A., and Locke, J. L. 1972, *Mem. R.A.S.*, 77, 109.

Minkowski, R. 1957, *IAU Symposium No. 4*, 107.

Misner, C. W., Thorne, K. S., and Wheeler, J. A. 1970, *Gravitation* (preliminary version).

Moffet, A. T. 1961, *Ph. D. Thesis*, California Institute of Technology.

Moffet, A. T. 1966, *Ann. Rev. Astr. and Ap.*, 4, 145.

Pacholczyk, A. G. 1970, *Radio Astrophysics*, (San Francisco: W. H. Freeman).

Palmer, H. P., Rowson, B., Anderson, B., Donaldson, W., Miley, G. K., Gent, H., Adgie, R. L., Slee, O. B., and Crowther, J. H. 1967, *Nature*, 213, 789.

Purcell, G. H. 1973, *Ph. D. Thesis*, California Institute of Technology.

Read, R. B. 1963, *Ap. J.*, 138, 1.

Rees, M. J. 1967, *M.N.R.A.S.*, 135, 345.

Rees, M. J. 1971, *Nature*, 229, 312.

Rogstad, D. H. 1968, *Applied Optics*, 7, 585.

Ryle, M. 1972, *Nature*, 239, 435.

Ryle, M. and Windram, M. D. 1968, *M.N.R.A.S.*, 138, 1.

Schmidt, M. 1963, *Nature*, 197, 1040.

Schmitt, J. L. 1968, *Nature*, 218, 663.

Seyfert, C. K. 1943, *Ap. J.*, 97, 28.

Shaffer, D. B., Cohen, M. H., Jauncey, D. L., and Kellermann, K. I. 1972, *Ap. J. (Letters)*, 173, L147.

Shapiro, I. I., Hinteregger, H. F., Knight, C. A., Punsky, J. J., Robertson, D. S., Rogers, A. E. E., Whitney, A. R., Clark, T. A., Marandino, G. E., Goldstein, R. M., and Spitzmesser, D. J. 1973, *Ap. J. (Letters)*, 183, L47.

Shimmins, A. J., Searle, L., Andrew, B. H., and Brandie, G. W. 1968, *Ap. Letters*, 1, 167.

Shklovskii, I. S. 1965, *Soviet Astr.—AJ*, 9, 22.

Terrell, J. 1966, *Science*, 154, 1281.

Van Vleck, J. H. and Middleton, D. 1966, *Proc. I.E.E.E.*, 54, 2.

Wade, C. M., Hjellming, R. M., Kellermann, K. I., and Wardle, J. F. C. 1971, *Ap. J. (Letters)*, 170, L11.

Whitney, A. R., Shapiro, I. I., Rogers, A. E. E., Robertson, D. S., Knight, C. A., Clark, T. A., Goldstein, R. M., Marandino, G. E., and Vandenberg, N. R. 1971, *Science*, 173, 225.

Wilkinson, P. N. 1972, *M.N.R.A.S.*, 160, 305.